Theoretical Description of the STM Images of Alkanes and Substituted Alkanes Adsorbed on Graphite

Francesco Faglioni,[†] Christopher L. Claypool,[‡] Nathan S. Lewis,[‡] and William A. Goddard III*,[†]

Materials and Process Simulation Center, Beckman Institute (139-74), and Division of Chemistry and Chemical Engineering, California Institute of Technology, Pasadena, California 91125

Received: January 7, 1997; In Final Form: April 16, 1997[⊗]

A theoretical model based on perturbation theory has been developed to predict the scanning tunneling microscopy (STM) images of molecules adsorbed on graphite. The model is applicable to a variety of different molecules with reasonable computational effort and provides images that are in qualitative agreement with experimental results. The model predicts that topographic effects will dominate the STM images of alkanes on graphite surfaces. The computations correlate well with the STM data of functionalized alkanes and allow assessment of the structure and orientation of most of the functionalized alkanes that have been studied experimentally. In addition, the computations suggest that the highly diffuse virtual orbitals of the adsorbed molecules, despite being much farther in energy from the Fermi level of the graphite than the occupied orbitals, may play an important role in determining the STM image contrast of such systems.

I. Introduction

The previous article[1] reports high-resolution scanning tunneling microscopy (STM) images of organic molecules adsorbed in ordered monolayers onto highly ordered pyrolytic graphite (HOPG) surfaces. The images reported therein reveal features as small as single atoms and/or functional groups in the adsorbed molecules and provide atomic level information on the electronic coupling profiles of such overlayers. The STM images observed in this work and in studies of related systems[2−5] are, however, dependent on subtle structural changes in the adsorbed molecules and appear to be the result of both electronic and geometric effects. Thus, to fully exploit this imaging technique, it is important to understand how different aspects of the adsorbate and the experimental conditions blend together to create the observed images.

In order to study and explain such phenomena for a large number of molecules, this article describes a theoretical model that has been developed to simulate the STM process. The method is accurate enough to be useful and reliable, it is simple enough to provide a facile method for interpretation of the available STM results, and it is cheap enough to be applicable to the systems of interest—small functionalized alkanes on HOPG—with affordable computational effort, e.g., a few hours on an HP9000 workstation.

In order to attain this goal, we have developed an alternative to expensive quantum mechanics computations that include explicitly the wave functions of the tip and/or the graphite. Our approach is to (1) use a force field (FF) to optimize the geometry of the adsorbed molecules on graphite, (2) determine the shapes and the energies of the molecular orbitals using Hartree−Fock (HF) computations for the isolated molecule, and (3) then simulate the STM image using a simple perturbative approach, which adds negligible cost with respect to steps 1 and 2.

Several theories have already been developed to predict and explain STM images of both surfaces and adsorbates. Tersoff and Hamman[6] used the transfer Hamiltonian approach first introduced by Bardeen.[7] Their conclusion is that the observed current is proportional to the local density of states (LDOS) at the Fermi energy of the sample, at the position of the tip. Adsorbates are observed through the change they induce in the LDOS of the support. Lang[8] replaced the support and the tip with the jellium model and used a metal atom to mimic the tip. This procedure was used to predict the images of adsorbed atoms using the transfer Hamiltonian approach in the low bias limit. Doyen and co-workers[9] have used semiempirical techniques to study the exact tunneling current, evaluating the interactions between the tip and the support explicitly and without the assumptions of the transfer Hamiltonian. More recently Hallmark, Chiang, and co-workers[10] have used extended Hückel calculations to predict images of aromatic molecules adsorbed on a metal substrate, and Sautet[11] used electron scattering techniques for the same purpose. Liang *et al.*[2] have also used the extended Hückel method to investigate the STM images of alkanes on graphite. Fisher and Blöchl[12] instead have performed *ab initio* density functional theory studies to simulate the STM imaging of adsorbed benzene molecules on graphite and MoS_2. Hui, Marcus, and Källebring[13] have developed a model for STM imaging of adsorbed molecules that includes the effect of *d* orbitals on the tip.

The models based on the transfer Hamiltonian have proven effective in predicting images of conducting surfaces in the low bias limit. Tersoff−Hamman theory has been used to interpret atomic resolution STM images of insulating molecules on a metallic substrate, and these studies have indicated that the molecular features of the images are determined by the most protruded atoms of the adsorbed molecules.[2,5] In addition, this work indicated that the insulating molecules were detected because their orbitals mix slightly into the Fermi level of the metallic substrate and because they are close to the tip.[2,5] When adsorbed insulating molecules are sampled with higher biases, this approach requires that the periodic molecular structure, as well as the supporting graphite, be included in the simulation.[2,12] As a result, significant effort is spent computing the band structure of the graphite every time a new molecule is studied. The method then becomes as complex as other approaches that can lead, in principle, to an exact prediction but are not based

* To whom correspondence should be addressed.
† Beckman Institute.
‡ Division of Chemistry and Chemical Engineering.
⊗ Abstract published in *Advance ACS Abstracts,* June 15, 1997.

S1089-5647(97)00180-6 CCC: $14.00

on the transfer Hamiltonian approximation. The result is that most methods that include the detailed wave functions of the graphite and the tip give excellent results but require extensive computations.

The goal of our work was to develop a theoretical approach that could aid in the interpretation of the experimental images obtained for alkanes and alkanols on graphite, in which the overlayer only is observed at high tip/sample biases.[1−3] Of course, the states of the graphite and of the tip are the initial and final states for tunneling processes for all of these molecular overlayers on a graphite surface. However, the primary goal of this theoretical study was to gain insight into the relative contributions of topographic and electronic factors in determining the STM contrast of different functional groups in the molecular overlayer. Since the experimental images for the different overlayers were obtained at a relatively constant tip/sample bias, the theoretical treatment focused on describing the changes in STM contrast for the various different molecules. To achieve this goal, a simple model was built that ignores the shape of the graphite states and that considers the coupling, or perturbation, between molecular states and a simplified version of graphitic states. In the high bias limit, such a model is expected to produce, at a fraction of the cost, the same results as a more complete treatment that explicitly includes the graphite orbitals. Of course, in the low bias limit, and for intermediate bias situations, this model will not be computationally useful nor physically appropriate. Our approach does, however, allow simulations of STM images on reasonably big systems with a good description of the molecular states involved mediating the tunneling process.

In section II we present the theoretical model and the approximations used to implement it. Section III then describes the predictions of the model and compares model and experiment for a number of molecules for which the experimental images have been obtained.

II. Theoretical Model

We are interested in determining how the electric current between a tip and a graphite support is modulated by one molecule adsorbed on the graphite. In the cases of concern, the molecules are physisorbed onto the graphite via van der Waals interactions. These interactions are small compared to the intramolecular forces, since van der Waals forces are typically on the order of 1 kcal/mol per pair of atoms, while bond energies are on the order of 100 kcal/mol per bond. Thus, the shape of the molecular wave function for the adsorbed molecule is not expected to change significantly relative to that of the unadsorbed molecule. Also, the interaction between the tip and the molecule must be small; otherwise the molecule would be displaced by the tip, and it could not be observed in the experimental STM image. The orbital energies, on the other hand, are expected to be affected by the presence of two conductors in close proximity to the molecule. According to classical electrostatics, the presence of the conductors results in a shift of the ionization potentials and electron affinities of the molecule, as described in section II.E.

II.A. Formalism. We will use the symbol $|t\rangle$ to describe the wave function of the tip. $|t\rangle$ belongs to a continuum of states with energies E_t and with a density of states $\rho_t(E_t)$. E_t^f indicates the Fermi energy of the tip. Similarly, $|g\rangle$ indicates the wave function of the graphite support, with E_g, $\rho_g(E_g)$, and E_g^f defined as the correponding energy, density of states, and Fermi energy, respectively. Also, the adsorbed molecule is described by its molecular orbitals $|k\rangle$ (and occasionally $|l\rangle$) having orbital energies E_k (E_l).

When a potential E_b, equivalent to a bias $-E_b$, is applied to the graphite support, electrons may flow from the more negative to the more positive side of the tunnel gap. When $E_g^f + E_b > E_t^f$, the electrons will flow from the states with energy $E_g \in (E_t^f, E_g^f + E_b)$ on the graphite to the states with energy $E_t \in (E_t^f, E_g^f + E_b)$ on the tip. The reverse is true when $E_g^f + E_b < E_t^f$. Throughout the article, the energy band into which the electrons are transferred under such a bias is denoted as the conduction region.

II.B. Coupling Potential. The perturbative potential, V, is the effective potential experienced by an electron in the region of space occupied by the molecule. Within the independent particle approximation, this potential is due to the Coulomb attraction of the nuclei, the average Coulomb repulsion from the molecular electrons, and the exchange interaction (from the Pauli principle).

V is exactly the potential used to solve the Hartree−Fock equation for the isolated molecule, so it acts on the molecular orbitals k as described in eq 1:

$$V^{\mathrm{HF}}|k\rangle = (H^{\mathrm{HF}} - T)|k\rangle = (E_{\mathrm{k}} - T)|k\rangle \tag{1}$$

where E_k is the orbital energy from the HF computation, T is the kinetic energy operator and H^{HF} is the Hartree−Fock Hamiltonian.

We are interested in tunneling conditions corresponding to the experimental observations, for which the molecules dominate the STM image contrast. This observation indicates that the direct coupling between the tip and the graphite is much smaller than the coupling through the molecular states. Thus it is legitimate to neglect the direct coupling of tip and graphite and to consider only the coupling through the molecular orbitals. This is equivalent to assuming that the unperturbed states of both tip and graphite overlap with the molecular wave function but not with each other. We also assume that there is no coupling between different states on the tip or on the graphite.

In this case, evaluation of all the relevant matrix elements for the coupling potential is readily performed:

$$\begin{aligned}
&\langle t|V|g\rangle = 0 && \text{assumed}\\
&\langle t|V|k\rangle = E_k S_{tk} - T_{tk} && \text{from eq 1}\\
&\langle g|V|k\rangle = E_k S_{gk} - T_{gk} && \text{from eq 1}\\
&\langle k|V|k'\rangle = 0 && \text{because the MOs are HF solutions}\\
&\langle t|V|t'\rangle \approx 0 && \text{assumed}\\
&\langle g|V|g'\rangle \approx 0 && \text{assumed}
\end{aligned} \tag{2}$$

where S and T are the overlap and kinetic energy matrices, respectively.

II.C. Perturbation Theory: Nondegenerate Case. The tunneling probability will be evaluated through the use of time-independent perturbation theory.[14] When the perturbation is off, the tip, molecule, and graphite do not interact. Thus, the unperturbed eigenstates are the functions $|t\rangle$ and $|g\rangle$ for the tip and the graphite along with the molecular orbitals $|k\rangle$ for the molecule. In the presence of the perturbation, the tip wave function is corrected by the first-order term of (3),

$$|t^{(1)}\rangle = \sum_k \frac{V_{kt}}{(E_t - E_k)}|k\rangle \tag{3}$$

and by the second-order term of (4),

$$|t^{(2)}\rangle = \sum_k \frac{V_{gk}V_{kt}}{(E_t - E_k)(E_t - E_g)}|g\rangle - \frac{1}{2}\sum_k \frac{|V_{kt}|^2}{(E_t - E_k)^2}|t^{(0)}\rangle \tag{4}$$

The first correction due to the function $|g\rangle$ appears in the second-order term. It is as if the functions $|t\rangle$ and $|g\rangle$ were coupled to first-order by the effective element:

$$\nu_{tg} = \sum_k \frac{V_{gk}V_{kt}}{(E_t - E_k)} \tag{5}$$

To first-order, this matrix element will be responsible for the tunneling current.

According to the Fermi golden rule, the number of transitions per unit time $d\omega_{gt}$ between an initial state $|t\rangle$ and all final states $|g\rangle$ with energy between E_g and E_g+dE_g is[14]

$$\mathrm{d}\omega_{gt} = \frac{2\pi}{\hbar}|\nu_{tg}|^2\delta(E_t - E_g)\,\rho_g(E_t)\,\mathrm{d}E_g \tag{6}$$

The total current is then

$$I_{gt} = \frac{2\pi}{\hbar}\int \rho_t(E_t)\,\mathrm{d}E_t \int \rho_g(E_g)\,\mathrm{d}E_g \left|\sum_k \frac{V_{gk}V_{kt}}{(E_t - E_k)}\right|^2 \delta(E_t - E_g) \tag{7}$$

$$= \frac{2\pi}{\hbar}\int \left|\sum_k \frac{V_{gk}V_{kt}}{(E - E_k)}\right|^2 \rho_t(E)\,\rho_g(E)\,\mathrm{d}E \tag{8}$$

where all integrals are over the conduction region. A more detailed description of the bias dependence is given in Appendix A.

This approach provides an alternate method, relative to the traditional transfer Hamiltonian formalism,[6,7] for obtaining an expression for the tunneling current under our conditions. In the transfer Hamiltonian formalism,[6] the graphite wave function includes explicitly the contributions from the molecular states.[2] Its coupling with the tip is due, in the high bias limit, mainly to these contributions. In our approach, the same physical picture is described, but within the framework of a perturbation theory formalism. The results are thus consistent with the transfer Hamiltonian theory and help to gain insight into the STM process of concern in the experimental data by focusing on the properties due to molecular states.

It should be noted that the common assumption that all of the STM current flows to or from states near the graphite Fermi level[2] does not hold in the high bias regime. The current involves all the states in the conduction region; hence an integration over energy in this region is required. This integration was performed for all of the molecular overlayers investigated during the course of this study.

II.D. Perturbation Theory: General Case. The above theory holds only for the case when all the energy differences in the denominators are large with respect to the coupling elements in the numerators. A more general treatment is described in this section. The molecular spectrum can be considered as a continuum with the following distribution:

$$S(E) = \sum_k V_{gk}V_{kt}\delta^{(\epsilon)}(E - E_k) \tag{9}$$

where $\delta^{(\epsilon)}(x)$ is such that

$$\lim_{\epsilon\to 0} \delta^{(\epsilon)}(x) = \delta(x) \tag{10}$$

and ϵ is a small quantity with the physical meaning of uncertainty in the energy. For instance, $\delta^{(\epsilon)}(x)$ can be taken to be a square function centered at $x = 0$ of width ϵ and height $1/\epsilon$.

It is now necessary to estimate the order of magnitude of ϵ. Whenever one of the orbitals falls in the conduction region, it is expected to be responsible for most of the observed current. A typical current used in STM imaging is 650 $pA = 9.8 \times 10^{-8}$ au, so on average one electron leaves the orbital to contribute to the current every $1/9.8 \times 10^{-8} \approx 1 \times 10^7$ au of time. If we further assume that the orbital is doubly occupied half of the time, then each electron spends about 5×10^6 au of time in the orbital; that is, the state with the electron in the orbital has an average lifetime of 5×10^6 au, which implies an uncertainty in its energy of $\hbar/(5 \times 10^6) = 2 \times 10^{-7}$ hartrees. Thus, a very rough order-of-magnitude estimate gives $\epsilon \approx 2 \times 10^{-7}$ and yields $\delta^{(\epsilon)}(0) \approx 5 \times 10^6$ au.

The number of transitions per unit time is then[14]

$$\mathrm{d}\omega_{gt} = \frac{2\pi}{\hbar}\left|\int \frac{S(E)}{(E_t - E + i0)}\mathrm{d}E\right|^2 \delta(E_t - E_g)\,\rho_g(E_t)\,\mathrm{d}E_g \tag{11}$$

where the notation $i0$ indicates that in evaluating the integral, one must take the principal value plus half the contribution from the residue on the integration path:

$$\int \frac{S(E)}{(E_t - E + i0)}\mathrm{d}E = P\int \frac{S(E)}{(E_t - E)}\mathrm{d}E + i\pi S(E_t) \tag{12}$$

Since ϵ is small, the integral can be computed easily. When all orbitals are not degenerate with the tip, this expression becomes the same as the one found for the nondegenerate case. When one of the orbitals, for example $|l\rangle$, is degenerate with the tip, its contribution to the principal value of the integral vanishes, so the integral becomes

$$\int \frac{S(E)}{(E_t - E + i0)}\mathrm{d}E = \sum_{k\neq l} \frac{V_{gk}V_{kt}}{E_t - E_k} + i\pi V_{gl}V_{lt}\delta^{(\epsilon)}(0) \tag{13}$$

The number of transitions per unit time due to the degenerate orbital is then

$$\mathrm{d}\omega_{gt} = \frac{2\pi}{\hbar}\pi^2|V_{gl}V_{lt}|^2[\delta^{(\epsilon)}(0)]^2\,\delta(E_t - E_g)\,\rho_g(E_t)\,\mathrm{d}E_g \tag{14}$$

The actual formula for the current is therefore

$$I \propto \int_{\mathrm{CR}} \rho_t(E)\,\rho_g(E)\left|\sum_{k\notin \mathrm{CR}} \frac{V_{gk}V_{kt}}{(E - E_k)} + i\pi \sum_{k\in \mathrm{CR}} V_{gk}V_{kt}\delta^{(\epsilon)}(E - E_k)\right|^2 \mathrm{d}E \tag{15}$$

where CR indicates the conduction region. Expanding the absolute value yields the desired expression:

$$I \propto \int_{\mathrm{CR}} \rho_t(E)\,\rho_g(E)\left\{\left[\sum_{k\notin \mathrm{CR}} \frac{V_{gk}V_{kt}}{(E - E_k)}\right]^2 + [\pi \sum_{k\in \mathrm{CR}} V_{gk}V_{kt}\delta^{(\epsilon)}(E - E_k)]^2\right\} \mathrm{d}E \tag{16}$$

where again the bias dependence (described explicitly in Appendix A) is included implicitly into the energy terms of (16).

II.E. Practical Implementation. Several other approximations were made in order to simplify the practical implementation of this approach. These are described below.

First, the tip wave function was replaced by a single 2*s* oxygen orbital (using the STO-3G basis).[15] This orbital is

similar in size to one lobe of a platinum d_{z^2} orbital, which would be the dominant orbital in computing the tip sample wave function overlap properties in a more complete quantum mechanical representation of the tip.

Second, the graphite wave function was replaced by an array of *2p* carbon orbitals (STO-3G basis) that were centered onto a grid of points. The coupling between the graphite and each MO was obtained by summing the absolute contributions from each lobe on the grid. Tests with various grid spacings gave essentially identical results. This choice of graphite basis set is one of several possible methods to implement practically our algorithm. As long as the wave function decay with distance is reasonable and coupling is allowed to occur to all of the graphite states, the result is expected to depend little on the actual form of the graphite wave function, especially when the features of interest are the relative functional group contrasts of the various molecular STM images under high bias conditions.

The grid used in the simulation was deliberately chosen to be more dense than the carbons on the real graphite surface in order to avoid accidental couplings that might arise due to the position of the grid.

Third, since the continuum and the discrete states cannot be easily normalized using the same criteria, the unnormalized states were used for the continuum part. As a consequence, all coupling elements are only known up to a proportionality constant. Thus, the actual current cannot be estimated at each tip position, but only the ratio between currents at different points is obtained.

This is not a practical drawback at the present time since only the relative tunneling probabilities are of primary interest in modeling the observed image contrast. This approach does have the disadvantage that it requires tuning the tip−molecule distance based on the experimental images rather than on the intensity of the current. This approximation is a limitation to the method that could, in principle, be removed by explicitly taking into account the proper normalization of the continuum states. We prefer to keep the model as simple as possible and thus have not pursued such refinements at the present time.

Fourth, the orbital energies of the MOs used in (16) were shifted to account for the presence of two conductors in close proximity to the molecule. This required an estimate of the Coulomb term acting on the molecular state. Within the HF framework, the energy of an occupied orbital has the physical meaning of an ionization potential: $E_{occ} = -IP = E_{molecule} - E_{cation}$. The presence of the conductors has little effect on $E_{molecule}$, but it stabilizes the cation; therefore E_{occ} becomes less negative, and the ionization potential decreases. Another way to view this effect is the following: in vacuum, the IP is the energy needed to move one electron from the molecule to infinity, whereas in the presence of the conductors, the electron must be moved only from the molecule to the conductor; therefore the IP decreases.

The stabilization effect can be computed with the method of image charges. Let the charge on the molecule be localized at its center of mass. The center of mass is estimated to be roughly halfway between the tip and the graphite, which, for this purpose, are taken to be two semi-infinite conductors terminated by two parallel planes.

Let R be the distance between the two planes and $R/2$ the distance between each plane and the localized charge. In order for the potential to be zero on the surfaces of the conductors, a first pair of negative charges can be placed at a distance $R/2$ into each conductor. Each one of these charges will have positive images at a distance $3R/2$ into the opposite conductor, and so on, to infinity, as depicted in Figure 1.

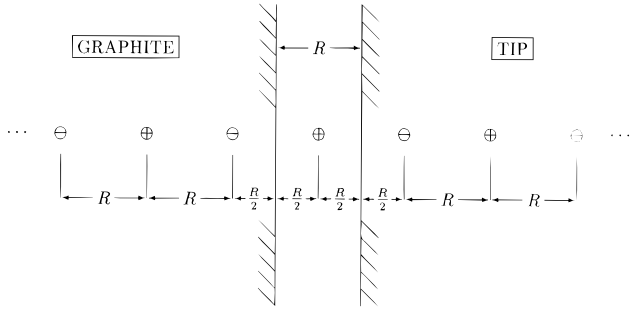

Figure 1. Charge distribution used to estimate the effect of the conductors on the orbital energies of the adsorbed molecule with the method of image charges. The molecular ion is replaced by a point charge halfway between the tip and the graphite, seen as semi-infinite conductors. R is the tip−graphite distance.

The electrostatic stabilization of the original charge due to this series of images is (in au)

$$\Delta E = 2\left\{-\frac{1}{R}+\frac{1}{2R}-\frac{1}{3R}+...\right\} = \frac{2}{R}\sum_{n=1}^{\infty}\frac{(-1)^n}{n} = -\frac{2\log(2)}{R} \quad (17)$$

Thus, the occupied orbital energies used in the computation of the current are shifted by adding $2\log(2)/R$, where R is the distance between the tip and the graphite.

The HF virtual orbitals, on the other hand, describe the energy required to add an electron to the molecule and thus have the physical meaning of electron affinities: $E_{virt} = E_{anion} - E_{molecule}$. In this case, the anion is stabilized by the presence of the two conductors, but the molecule is not, so the virtual orbital energies must be corrected by subtracting the quantity $2\log(2)/R$. This treatment is not rigorous, as we do not account for the different shapes and polarizabilities of different orbitals. However, it is very simple, and it gives a reasonable estimate of this Coulombic correction term.

The different behavior of occupied and virtual orbitals is a consequence of the definition of orbital energy arising from the HF treatment. All HF orbital energies include the interactions of an electron in the orbital with the nuclei and with all the other electrons in the system. For a molecule containing N electrons, for instance, the energy of an occupied orbital includes interactions with the remaining $(N - 1)$ electrons while the energy of a virtual orbital includes interactions with all N electrons. Occupied orbital energies, therefore, describe the removal and virtual orbital energies describe the addition of one electron with respect to the state for which the orbitals were optimized.

Fifth, orbitals that fall in the conduction region must be treated separately. During the flow of current their occupations and their orbital energies are not easily defined. A simple approximation is to assume that these orbitals fall in the middle of the conduction region. Notice also that orbitals that are occupied in the isolated molecule, but that fall above the conduction region, are not well-described and hence should be treated as conduction orbitals.

Sixth, it is necessary to estimate the potential distribution when a bias is applied across the tip−sample gap. When the tip, molecule, and graphite are brought together, the Fermi levels of the three components tend to become equal at the interface.[16] The rigorous description of this effect is rather complicated, requiring sophisticated computational techniques that would considerably increase the cost of the simulation. For the situation of interest, the Fermi energies of the metal tip and of

TABLE 1: Ionization Potentials (eV)

molecule	IP[a] (Koopmans')	IP[b] (HF)	IP[c] (MP2)	IP[d] (exptl)
$CH_3(CH_2)_4CH_3$	11.57	10.12	10.44	(10.22)[e]
$CH_3(CH_2)_3OH$	11.87	9.24	10.56	10.37−10.44
$CH_3(CH_2)_3F$	12.53	11.10	11.30	*f*
$CH_3(CH_2)_3Cl$	11.42	9.96	10.60	10.84
$CH_3(CH_2)_3Br$	10.55	9.38	9.75	(10.15)[e]
$CH_3(CH_2)_3I$	9.62	8.66	8.99	9.5
$CH_3(CH_2)_3CN$	11.92	10.48	12.05	*f*
$C_2H_5CF_3$	14.02	12.85	12.72	*f*
$C_2H_5COC_2H_5$	11.14	7.97	9.55	9.52
$C_2H_5NHC_2H_5$	9.87	7.37	8.54	8.63−8.68
$C_2H_5NH_2$	10.47	8.19	9.33	9.47−9.50
$C_2H_5OC_2H_5$	11.32	8.46	9.85	9.59−9.70
$C_2H_5SC_2H_5$	9.00	7.44	8.23	7.45−8.44
C_2H_5SH	9.60	8.21	8.94	(9.15)[e]
$C_2H_5SSC_2H_5$	9.13	8.06	8.15	8.70−8.85
CH_3COOH	11.90	8.78	10.35	(10.66)[e]
$C_2H_5CCC_2H_5$	9.37	7.90	9.14	(9.32)[e]
$C_2H_5CHCHC_2H_5$	8.74	7.35	8.69	9.14

[a] Estimated based on Koopmans' theorem (HF orbital energy) with 6-31G** basis set. [b] Estimate obtained by comparing the total HF/6-31G** energies of the molecule and the cation. [c] Estimate obtained by comparing the total MP2/6-31G** energies of the molecule and the cation. [d] Experimental value from ref 24. [e] Adiabatic ionization potential. [f] Data not available.

the graphite were assumed to be equal to each other. Additionally, as derived previously, the bias was assumed to be distributed in the tip−sample gap such that the molecule experiences half of the bias potential.[1,17]

To account for the effects of the initial charge equilibration on the energies of the molecular orbitals, all orbital energies were considered to be shifted from their values in vacuum by an amount λ. This quantity represents the difference between the computed HF orbital energies, rescaled to account for the presence of the conductors, and the real orbital energies of the adsorbed molecules during the STM imaging experiment.

λ includes contributions from two very different phenomena. One contribution to λ arises from the inability of HF calculations to reliably predict ionization potentials. This contribution can be evaluated by comparison of the HOMO energy obtained from the HF calculation to a reliable value for the ionization potential of the molecule, obtained either from experimental data or from high-level calculations. For a number of small moleculels, the energies of both the molecules and the corresponding cations were computed at the HF and MP2 level, and the resulting ionization potentials, as well as the experimental ones whenever available, are displayed in Table 1. Although the HOMO energy obtained from the HF calculation tends to overestimate the true ionization potential by about 1 eV, the error changes considerably for different molecules. The correction for this effect was estimated for every class of molecules, and this correction was included in the value of λ for each different molecule. For consistency, the value chosen for the correction was taken as the difference between the HF HOMO energy and the ionization potential that was computed at the MP2 level.

The other contribution to λ arises from a need to account for possible energetic differences between the energy levels of molecules adsorbed onto graphite and those in vacuum. It is likely that the reference energy for a molecule (the chemical potential of the electrons in the molecule) changes from its value in vacuum when the molecule instead is adsorbed on graphite, surrounded by solvent, and approached by the tip. For the substituted alkane chains under similar tunneling conditions (i.e. similar bias and tunneling current), this component of λ was chosen to best reproduce in general the entire set of observed images and then was not varied for calculations on individual systems.

Seventh, the density of states for the tip $\rho_t(E)$ was assumed to be a constant in the conduction region. The density of states for the graphite $\rho_g(E)$ was assumed to be a parabola having a vertex at the initial value of the graphite Fermi level,[18] $\rho_g(E) \propto (E - E_f)^2$.

Adopting these approximations, the STM current is then

$$I \propto \int_{CR}(E_f - E)^2\left[\sum_{k\notin CR}\frac{V_{gk}V_{kt}}{(E - E_k)}\right]^2 dE + \int_{CR}(E_f - E)^2[\pi \sum_{k\in CR} V_{gk}V_{kt}\delta^{(\epsilon)}(E - E_k)]^2\, dE \quad (18)$$

where again the bias dependence is implicitly contained in the energy terms of (18). The first of these integrals is computed numerically (e.g. using Simpson's rule), and the second one uses the estimates of E_k described above and the value of $\delta^{(\epsilon)}(E - E_k)$ obtained in section II.D.

II.F. General Procedure. For every chemical species, one molecule was laid onto a rigid graphite slab and the molecular geometry was optimized using the DreidingII FF[19] with charges estimated using charge equilibration.[20] Two more molecules were then added, parallel to the first one and sandwiching it, at a distance of about 4.5 Å. The molecular geometry was then reoptimized. The distance of 4.5 Å was chosen because it is close to the one observed experimentally, both in STM images[1] and in low-angle X-ray diffraction experiments of alkane and alkanol overlayers on HOPG.[21]

The central molecule was then isolated without changing its geometry. All alkyl chains were truncated four carbons away from any functional group, and the cleaved bonds were saturated with hydrogens. The resulting molecules were then checked for symmetry elements. The molecules that were found to be symmetric (with a tolerance of 0.04 Å) were symmetrized in order to speed up the Hartree−Fock computation. A standard HF computation was then performed on the resulting molecules using the 6-31G** basis set.[22] The choice of the basis set was motivated by the desire for reasonably accurate orbital energies.

To simulate an STM scan, a grid of 26 × 26 points was positioned to correspond to the graphite surface in the FF computation. All of the coupling elements with the graphite were then computed placing one carbon 2p orbital at each grid point. The tip was positioned on a grid of 51 × 51 points that was positioned parallel to, and at a fixed distance from, the plane of the graphite grid. For each position of the tip, the coupling elements were computed and the tunneling current was estimated assuming a bias of −1 eV. The resulting data were then used to produce three-dimensional plots or contour diagrams of the current. This approach simulates a constant height STM image and was used to calibrate the tip−graphite distance and to establish the value of the parameter λ. For each molecule, a constant current simulation was also performed, in which the tip was allowed to move in a direction perpendicular to the graphite in order to adjust the current to a fixed value. The tip displacement was then plotted with respect to an arbitrary plane that was parallel to the graphite surface. These simulations are 3−4 times more computationally expensive than the constant height simulations, but resemble more closely the experimental STM technique. Qualitative agreement was observed between the computed constant height and constant current images for all the cases studied in this work.

In order to facilitate interpretation of the results in terms of electronic and geometric effects, the overlap between the tip wave function and the occupied molecular orbitals was also evaluated. The resulting images have no experimental equivalent, but represent what the STM image would look like if only the geometry of the molecule were mapped while all electronic

effects were ignored. The comparison of these images with the results of the complete simulations will point out whether topographic or electronic effects are primarily responsible for the features that are observed in the experimental and computed STM images.

The tip−molecule distance that was used for the constant height simulations and the current used in the constant current simulations were each chosen to reproduce as closely as possible the features that were observed experimentally. A tip−molecule distance of 7 au (≈3.7 Å) was selected for the constant height simulations. At this distance, the maximal current observed for the alkane molecules is close to 0.001 arbitrary units (only relative current densities are computed in the present model), and this value was used for the constant current simulations. For much shorter distances, the resulting images seem to be determined mainly by the topology of the molecule, while at much longer distances the computed resolution decreased below that observed experimentally.

In all constant current plots, the tip was not allowed to get too close to the graphite, so these plots produce features that appear to be bumps on a flat surface. In previous simulations reported in the literature,[2] STM images have been related to the local density of states at a distance of 0.5 Å from the adsorbed molecule. We believe such distances are unrealistically small to describe actual STM measurements. In our work, the distance corresponding to the flat surface was set to be 14.5 bohrs for molecules oriented with their carbon−carbon skeletons parallel to the graphite surface plane and 15 bohrs for molecules having their carbon−carbon skeletons oriented perpendicualr to the plane of the graphite surface. These values correspond to a tip−molecule distance of about 2.9 Å.

The value of the parameter λ was chosen to best reproduce the experimental images. While the value of λ has little or no effect on most molecules, it plays a fundamental role for the molecules having their highest occupied molecular orbitals (HOMOs) close to the conduction region. After correcting for the difference between the HOMO orbital energy and the MP2 ionization potential, as reported in Table 1, the second contribution to λ was estimated by the value needed to bring the HOMO of the amines into the conduction region and to leave the HOMO of the alkyl bromide at lower energy. This condition is satisfied for any correction between 1.3 and 1.8 eV, assuming a tip−molecule distance of 7 au. We arbitrarily selected a correction of 1.5 eV. This value was fixed for all the simulations, on the basis that it should be approximately equal for all the molecules of concern.

III. Results

The orientation of the carbon−carbon skeletons of the alkyl chains relative to the graphite surface plane must be carefully considered in order to accurately model the STM images that have been observed experimentally. In the discussion that follows, the term flat will be used to indicate adsorption orientations in which the carbon−carbon skeleton of the alkane chain lies parallel to the plane containing the graphite surface, while the term vertical will be used to indicate the situation in which the carbon−carbon skeleton is oriented perpendicular to the graphite surface plane. Also, since the tip is assumed to be above the graphite, down and up will be used to describe atomic positions that are located toward the graphite and toward the tip, respectively.

III.A. Alkanes. To investigate the geometry and packing of adsorbed alkanes, the molecule $CH_3(CH_2)_{33}CH_3$ was considered, since it is the alkane that was imaged experimentally with the STM.[1] According to the results from the FF study, a single *trans*-$CH_3(CH_2)_{33}CH_3$ molecule adsorbs on graphite in the flat orientation, with the vertical orientation being less stable by 8 kcal/mol. The adsorption energy (from the gas phase) for $CH_3(CH_2)_{33}CH_3$ was computed to be on the order of 70 kcal/mol. In these computations, only the all *trans*-conformation was considered. This was justified because conformations with *gauche*-bonds were likely to be significantly less favorable energetically and because the experimental STM[1] and X-ray diffraction[21] data strongly suggest that the alkanes are adsorbed in an *all-trans*-conformation onto the graphite surface.

When three *trans*-$CH_3(CH_2)_{33}CH_3$ molecules are adsorbed from the gas phase, each pairwise interaction between neighboring molecules was computed to further stabilize the system by about 23 and 56 kcal/mol in the flat and the vertical orientations, respectively. Consequently, for a three-molecule overlayer model, the vertical orientation is computed to be more stable by an energy difference of 25 kcal/mol.

The experimental images indicate that the molecules are generally adsorbed in the flat orientation.[1,2] Although the vertical orientation is computed to be more stable, if the monolayer is built by adding one molecule at a time and by letting it migrate on the graphite surface, it is conceivable that the system would be trapped into the flat orientation. Migration of a single $CH_3(CH_2)_{33}CH_3$ molecule on the graphite surface was computed to have a barrier of 1−2 kcal/mol. However, the barrier to flip one $CH_3(CH_2)_{33}CH_3$ molecule into the vertical orientation is estimated to be around 18 kcal/mol, making this process unlikely at room temperature. This proposed nucleation process is similar to one that has been recently observed in an STM study of the growth dynamics of self-assembled thiol monolayers on gold.[23] An alternative possibility that was not explored in the present calculations is that since the adsorption occurs from solution, differential solvation plays a significant role in determining the energetically favored orientation of the molecules in the graphite overlayer.

Instead of carrying out more extensive simulations to include both dynamical effects and solvation effects, both orientations of the alkane were investigated in order to evaluate which produced computed STM images that more closely matched the experimental data. The images for $CH_3(CH_2)_7CH_3$ in the vertical orientation are reported in Figure 2A. The constant current image of Figure 2A clearly does not match the high-resolution STM image observed experimentally for alkanes on HOPG.[1] The constant height and the constant current images show spots corresponding to the hydrogens closest to the tip, leading to a rectangular pattern that is predominantly due to the geometry of the molecule, similar to the conclusions of a previous extended Huckel level analysis of this system.[2] Our calculations produced an average distance between maxima in the constant current mode of 2.59 Å in the direction along the backbone and an average distance of 1.57 Å between nearest neighbors.

The STM images predicted for the flat molecule $CH_3(CH_2)_6CH_3$ at a bias of −1 eV are reported in Figure 2B. The constant current and constant height images of the alkane in this orientation were similar to each other, and both displayed patterns that closely match the pattern produced by the geometric locations of the hydrogens that were closest to the tip. This effect can be seen more clearly by comparison of the image in Figure 2B to the overlap plot of Figure 2C. This comparison indicates that the molecular topography alone is sufficient to explain the qualitative aspects of the computed STM image of this system.

The images of Figure 2B are in excellent agreement with the experimental images obtained for alkanes on graphite.[1] In the constant current simulation, the average distance between subsequent spots along the alkane chain is 2.61 Å and the

(A) Vertical $CH_3(CH_2)_7CH_3$ at $-1.0\ eV$ Constant current

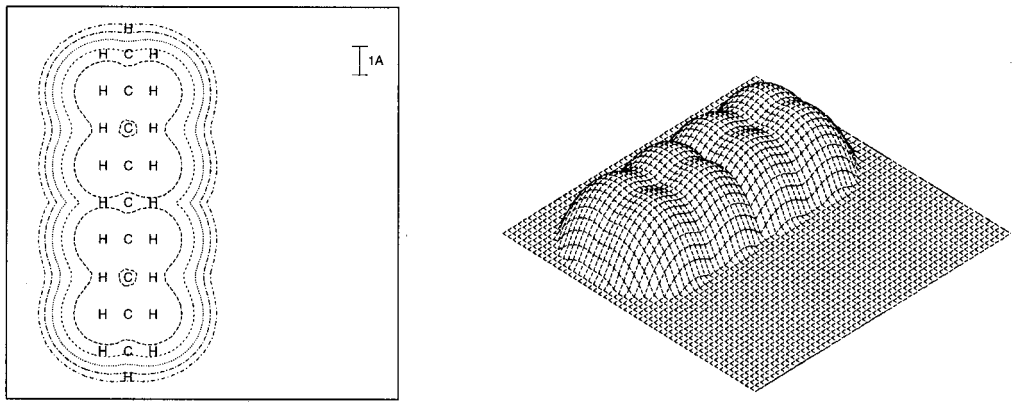

(B) Flat $CH_3(CH_2)_6CH_3$ at $-1.0\ eV$ Constant current

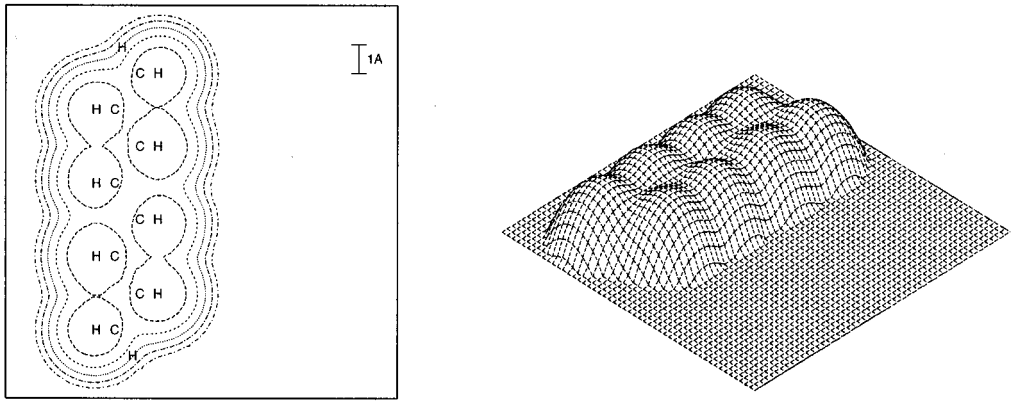

(C) Flat $CH_3(CH_2)_6CH_3$ at $-1.0\ eV$ Overlap Only

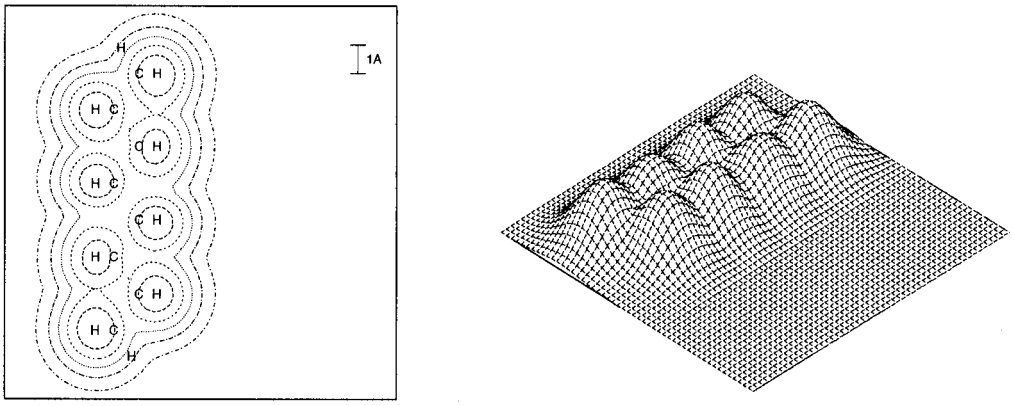

Figure 2. Computed STM images of an alkane molecule adsorbed onto the graphite surface. The contour levels are at 1/6, 2/6, 3/6, 4/6, and 5/6 of the maximum peak of each plot; the same spacing criteria for contour levels is used for all the contour plots of the paper. 3-D plots are shown to the right of the contour plots. The bias is −1 eV in all panels of Figures 2−16 unless otherwise noted. In A, the vertical orientation is assumed, while B and C depict results for the flat orientation. (A) Constant current simulation; the plot represents the tip displacement perpendicular to the graphite surface. The maximum displacement is 1.71 au. (B) Constant current simulation in the flat orientation. The maximum displacement is 1.47 au. (C) Simulation of only the overlap of the tip with the occupied MOs at each tip position (see text for details). The maximum current is 0.050 arbitrary units.

average distance between spots along the direction of the molecule is 2.56 Å, whereas the experimental data are 2.35 Å between spots along the chain and 2.54 Å between spots along the direction of the molecule. The positions of the spots observed experimentally are not in exact agreement with those in the simulation presumably due to the approximations contained in both the model and the computation.

It is also of interest to examine the relative contribution of the occupied and unoccupied orbitals to the overall tunneling current. Since the occupied orbitals of the alkane are very stable, the computations indicate that the current is determined mainly by the virtual orbitals. A simple interpretation of this behavior is that the tunneling electrons behave as low-energy electrons elastically scattered by the adsorbed molecules.

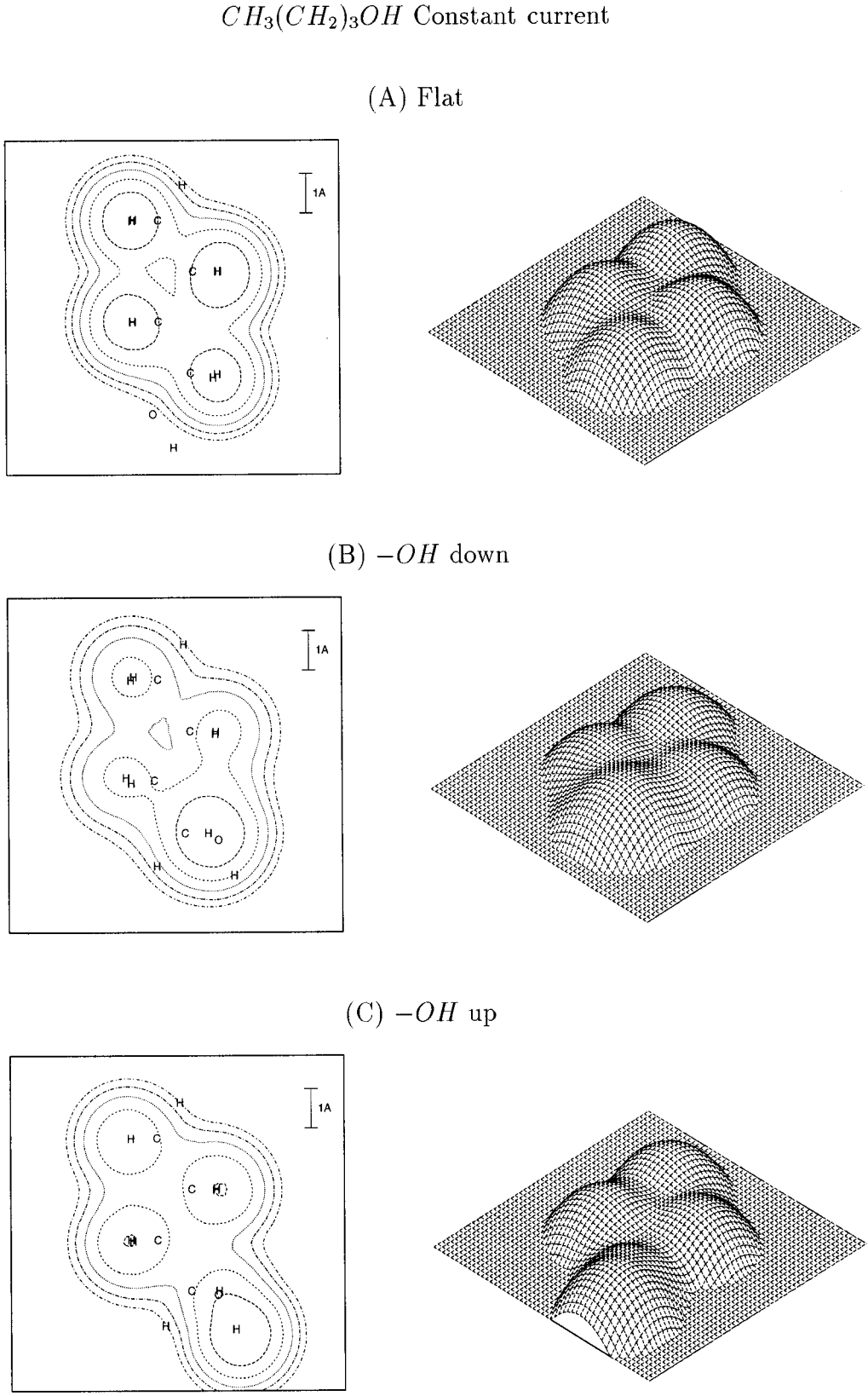

Figure 3. Computed constant current STM images of an alcohol molecule laid flat on the graphite surface. (A) The OH group is *trans* to the alkyl chain. The maximum value of the plot is 1.00 au. (B) The OH group is *gauche* to the alkyl chain and it points toward the graphite. (C) The OH group is *gauche* to the alkyl chain and it points away from the graphite. The maximum values of the plots in B and C are 1.32 and 1.12 au, respectively.

Because the same coupling is present in both biases, the images are predicted to be symmetric with bias voltage,[1,17] in accord with experimental observations.[1]

III.B. Alkanols. Since the experimental STM images show that alkanols lay flat on HOPG,[1] only the flat adsorption orientation was considered computationally for these systems. The molecular geometry of the adsorbed alkanol was computed for the molecule $CH_3(CH_2)_{11}OH$, and the *ab initio* computation of the STM image was carried out on the molecule $CH_3(CH_2)_3$-OH.

Three conformations were investigated for the flat orientation of $CH_3(CH_2)_{11}OH$ on graphite. For one adsorbed molecule, the

(A) $CH_3(CH_2)_3F$

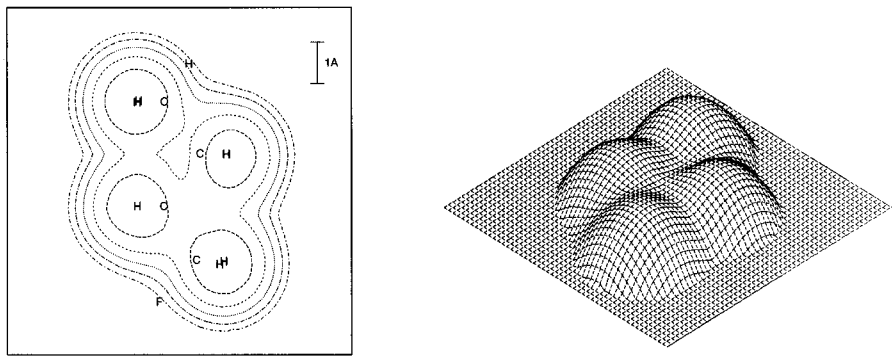

(B) $CH_3(CH_2)_3Cl$

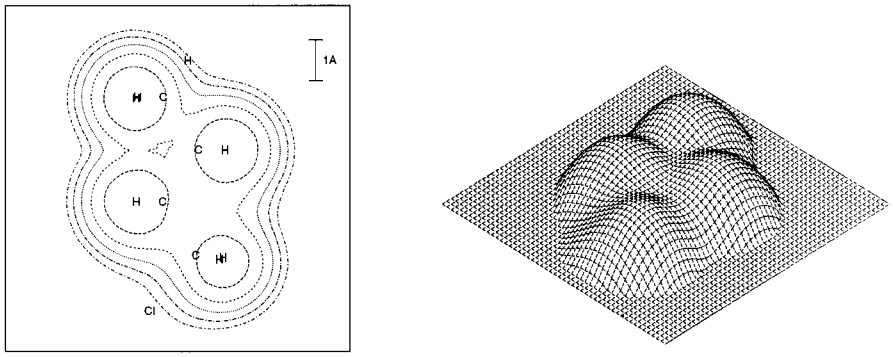

(C) $CH_3(CH_2)_3Br$

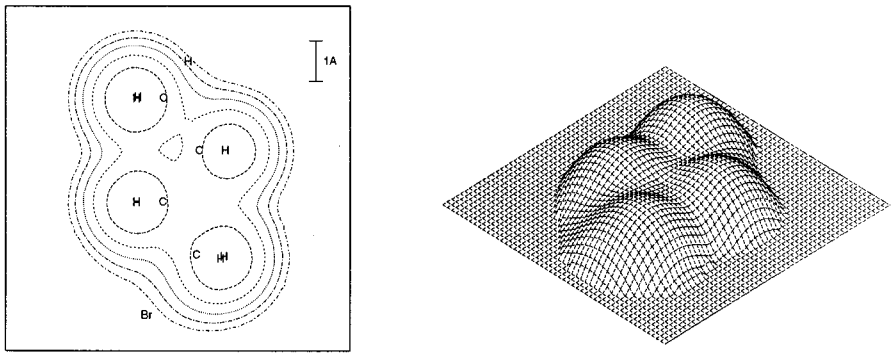

(D) $CH_3(CH_2)_3I$

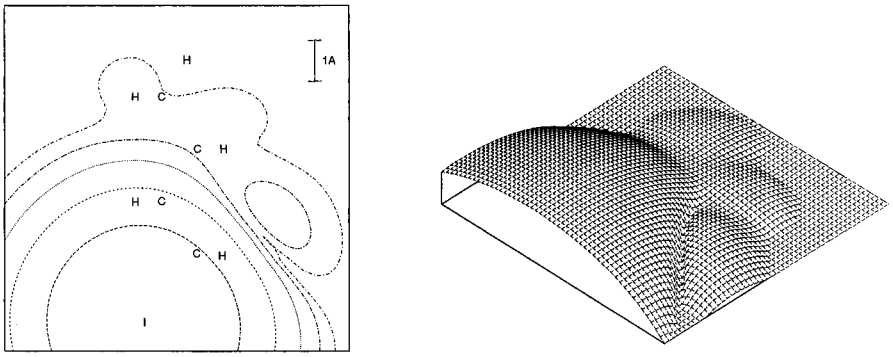

Figure 4. Computed constant current STM images of halobutanes laid flat on graphite: (A) fluorobutane; (B) chlorobutane; (C) bromobutane; (D) iodobutane. The maximum values for the plots are 0.99, 0.99, 0.98, and 5.16 au, respectively.

most stable conformation was the one with the OH group *trans* to the alkyl chain. This conformation was computed to have an adsorption energy of 26.3 kcal/mol from the gas phase. The two *gauche*-conformers, in which the OH group was either

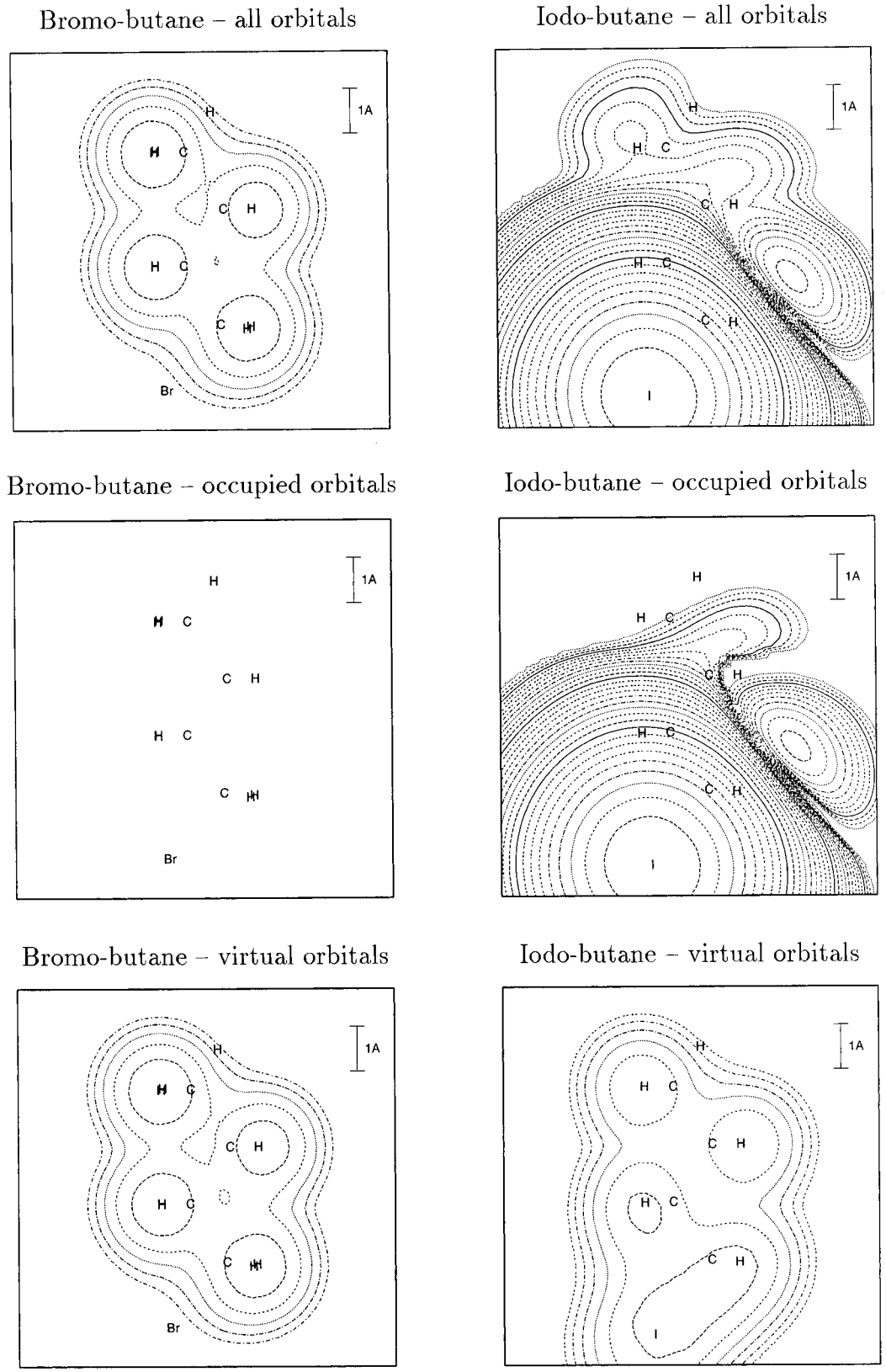

Figure 5. Computed STM images of bromo- and iodobutane in the constant current mode. The top two plots represent the total current transmitted. The contributions to the current due to the occupied (center) and the virtual (bottom) orbitals alone are reported to show the similarity between the two molecules. To illustrate the differences between the two molecules, the same contour levels and reference distance were used in all plots. Each contour line represents a tip displacement of 1/6 au. The zero corresponds to a tip−graphite distance of 14.5 au (i.e., a tip−molecule distance of about 2.9 Å), and only positive displacements are computed. In the bromine, the total current is dominated by the virtual orbitals, while in the iodine it is dominated by the occupied orbitals.

pointing toward the graphite (OH down) or toward the tip, denoted as OH up, were less stable by 3.4 and 3.0 kcal/mol, respectively. For three $CH_3(CH_2)_{11}OH$ molecules adsorbed on graphite, the *trans*-conformer was again the most energetically favored in the computations, while the *gauche*-conformers were 3.2 and 3.1 kcal/mol higher in energy, respectively.

Figure 3A displays the computed STM images for the most energetically favorable, *trans*-conformer of $CH_3(CH_2)_3OH$ at a

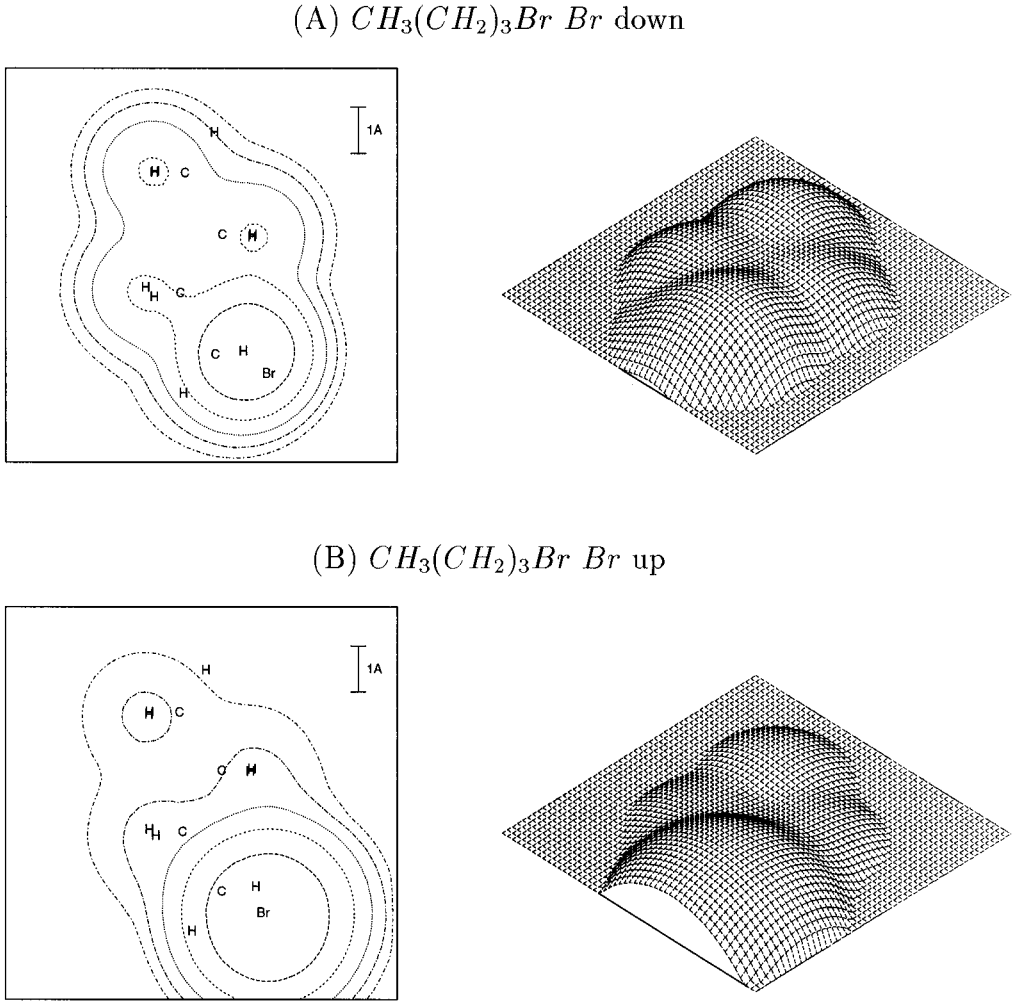

Figure 6. Computed constant current STM images of bromobutane on graphite. (A) The Br is *gauche* to the alkyl chain and points toward the graphite. (B) The Br is *gauche* to the alkyl chain and points away from the graphite. The maximum values in the plots are 1.91 and 2.95 au, respectively.

bias of −1 eV in the flat orientation. The simulation shows that the alcohol is dark with respect to the alkyl chain, in accord with experiment. Additionally, the image of the chain is dominated by the spots corresponding to the hydrogen atoms closest to the tip, as in the case of unsubstituted alkanes.

The average distance between spots is 2.63 Å along the direction of the molecule and 2.62 Å between nearest neighbors. The average angle between spots imaged on the alkyl chain is 60.2°. The experimental values for $CH_3(CH_2)_{13}OH$ are 2.57 Å, 2.36 Å, and 61°, respectively.[1] The difference between these computed values and the ones obtained for the unsubstituted alkane can be attributed to the fact that the alkyl chain used in the computational modeling of the alkanol overlayer is shorter and hence is less representative of the real system. Again the virtual orbitals were primarily responsible for the contrast between the OH group and the hydrogens in the methylene chain.

The *gauche*-conformers of the alkanol produced significantly different computed STM images. The OH group in the computed STM plot for both *gauche*-isomers is brighter than the spots in the alkyl chain, although the computations indicate that the oxygen atom is not observed directly by the STM for either conformation of the alkanol. For the OH down conformation, the α hydrogen is forced up toward the tip and becomes bright due to a topographic effect (Figure 3B). For the OH up conformation, the hydrogen atom of the OH group is close to the tip and is thus computed to be imaged as a bright spot (Figure 3C). Since the *gauche*-conformations produce computed images that do not agree with experimental observation, but the computed STM image of the *trans*-conformation does agree with the data, it is therefore reasonable to conclude that the more energetically favored *trans*-conformer was in fact being imaged experimentally in the work of Claypool *et al.*[1]

III.C. Halogenated Alkanols. For these molecules, only the flat orientation was considered. This was justified by the observation that the experimental images of halogenated alkanols show the same packing as that displayed by unsubstituted alkanols,[1] for which the high-resolution STM images clearly revealed a flat orientation.[1] The parameters of the adsorbed molecules were determined for $X(CH_2)_{12}OH$, where X = F, Cl, Br, and I, whereas the *ab initio* STM image computations were performed on the smaller molecules $X(CH_2)_3CH_3$.

Figure 4 depicts the images computed for these adsorbates at a bias of −1 eV. These images display the results obtained for the most energetically stable conformation, in which the halide was in a *trans*-conformation relative to the alkyl chain. The images show that the functional groups F, Cl, and Br appear dark in the STM images relative to the alkyl chain, while I is much brighter than any other part of the iodoalkanol. These predictions are in excellent agreement with the experimental observations.[1]

In the case of $(CH_3)(CH_2)_3I$, the two highest occupied molecular orbitals (HOMOs) fall in the conduction region. The molecule then becomes a conductor, and most of the current goes through the lone pairs on the iodine.

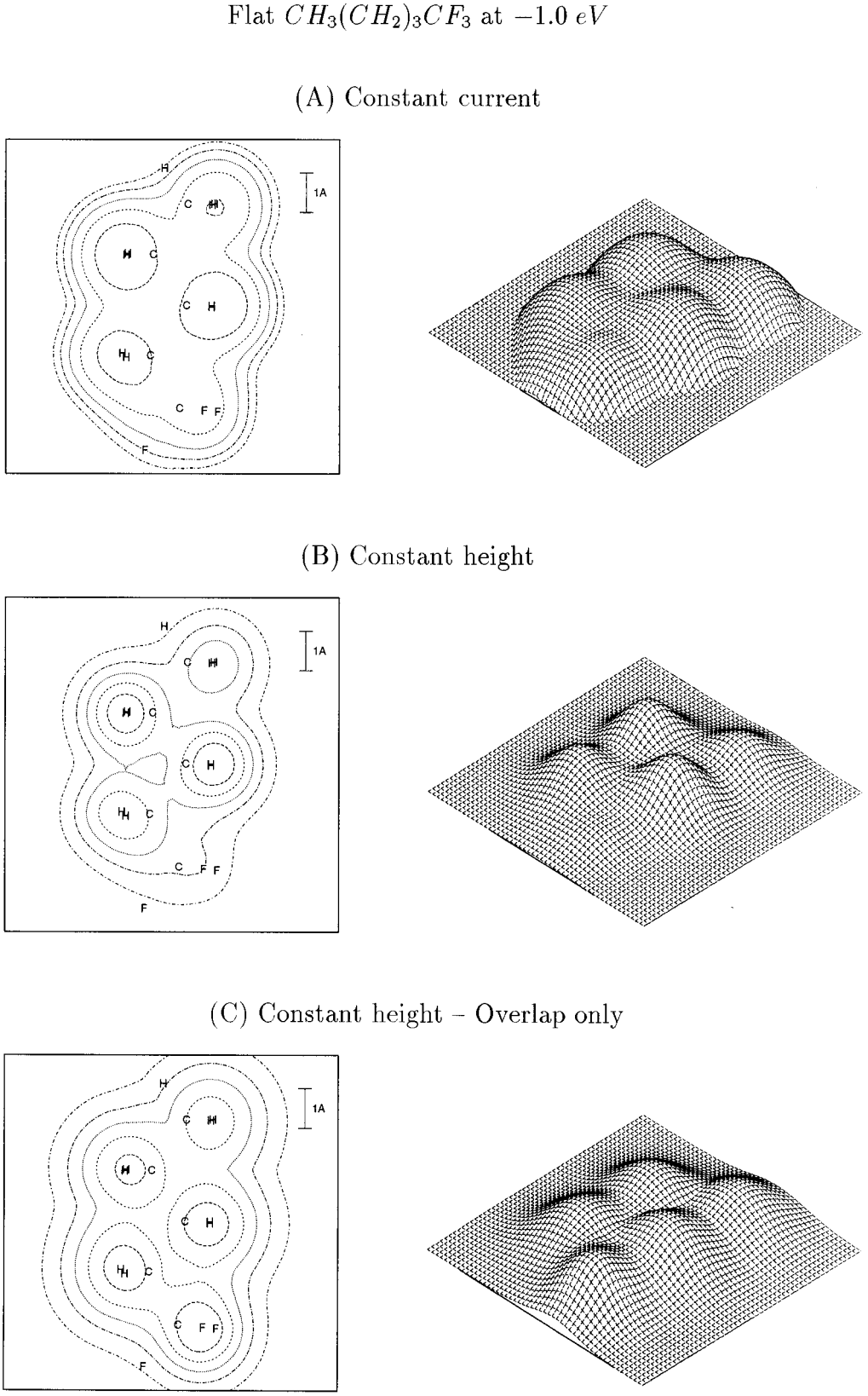

Figure 7. Computed constant current STM images of $CH_3(CH_2)_3CF_3$ laid flat on the graphite surface. The maximum values for the three plots are (A) 1.12 au; (B) 0.00038 arbitrary units; and (C) 0.054 arbitrary units.

In the case of $(CH_3)(CH_2)_3X$, with X = F, Cl, and Br, both the occupied and virtual orbitals are far in energy from the conduction region. As the virtual orbitals reach farther out from the molecule than the occupied orbitals, they couple better with the tip and with the graphite. Consequently, the virtual orbitals are computed to be responsible for most of the current. These halogens cannot transmit current and thus appear dark in the STM image contrast, because they have no low-energy virtual orbital available. To illustrate these effects, Figure 5 compares the constant current images obtained from the entire STM image computation to those computed for the alkyl bromide and alkyl iodide adsorbates when only the occupied or the virtual orbitals are considered. When only the occupied orbitals are considered, both Br and I are bright, even though I is much brighter.

Computations were also performed for two other conformations of the alkyl bromide, both of which had the Br in a *gauche-*

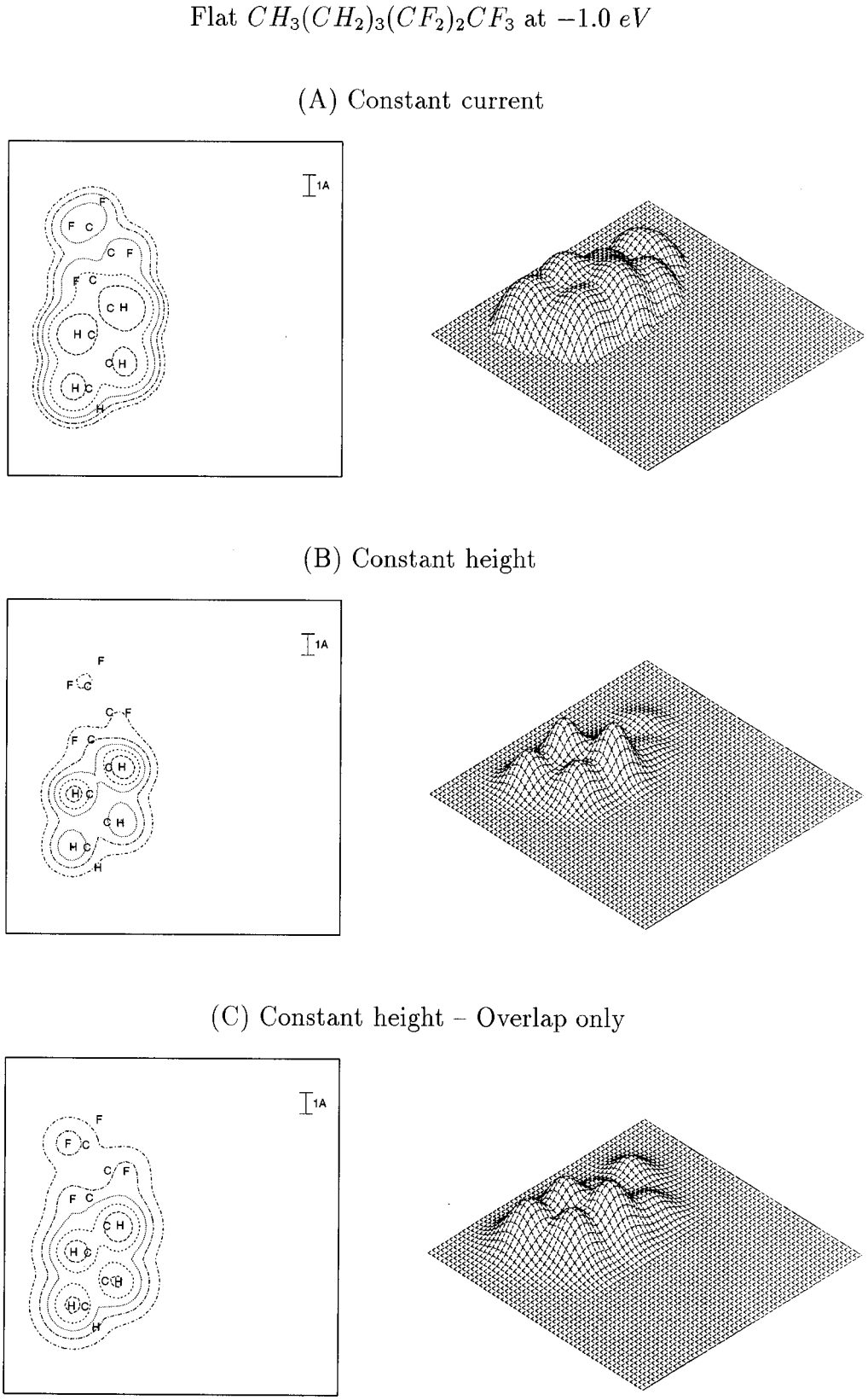

Figure 8. Computed constant current STM images of $CH_3(CH_2)_3(CF_2)_3CF_3$ laid flat on the graphite surface. The maximum values for the three plots are (A) 1.55 au; (B) 0.0011 arbitrary units; and (C) 0.097 arbitrary units.

position relative to the alkyl chain. In one conformation, the Br group was pointing toward the graphite (Br down), and in the other conformation the Br was pointing away from the graphite (Br up).

For a single adsorbed molecule, the adsorption energy (from the gas phase) of the *trans*-Br conformation was 28.9 kcal/mol, whereas the *gauche*-conformers were found to be less stable by 3.6 kcal/mol (Br down) and 3.5 kcal/mol (Br up). For three adsorbed molecules, the *gauche*-conformers were less stable than the *trans* by 11.9 kcal/mol (Br down) and 13.7 kcal/mol (Br up).

STM simulations were performed on both of these *gauche*-conformations. As displayed in Figure 6, changing the conformation from a *trans*- to a *gauche*-alkyl halide is predicted

$$CH_3(CH_2)_3O(CH_2)_3CH_3$$

(A) Vertical, *O* down

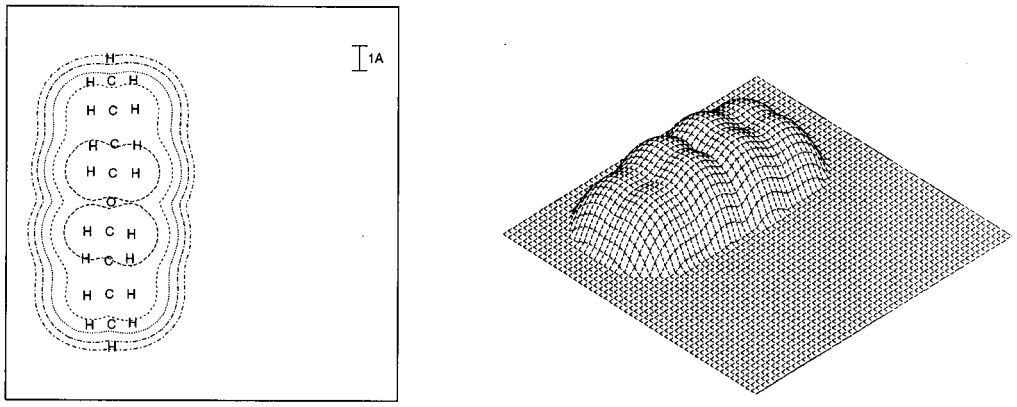

(B) Flat

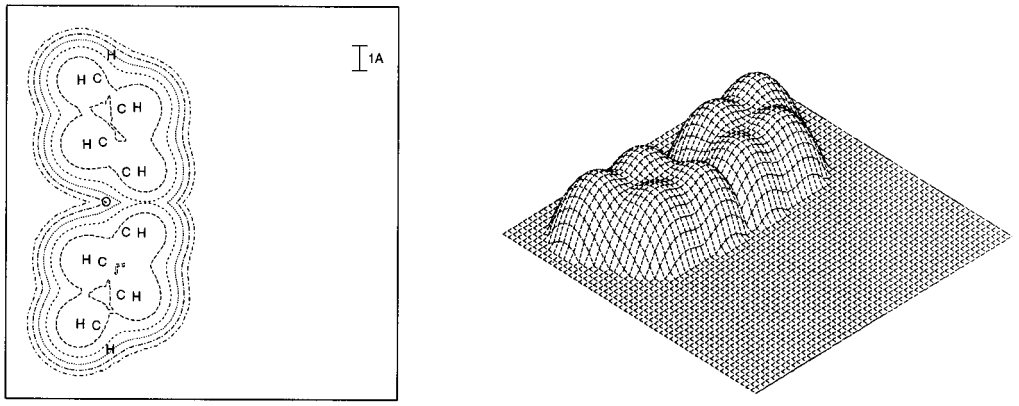

(C) Vertical, *O* up

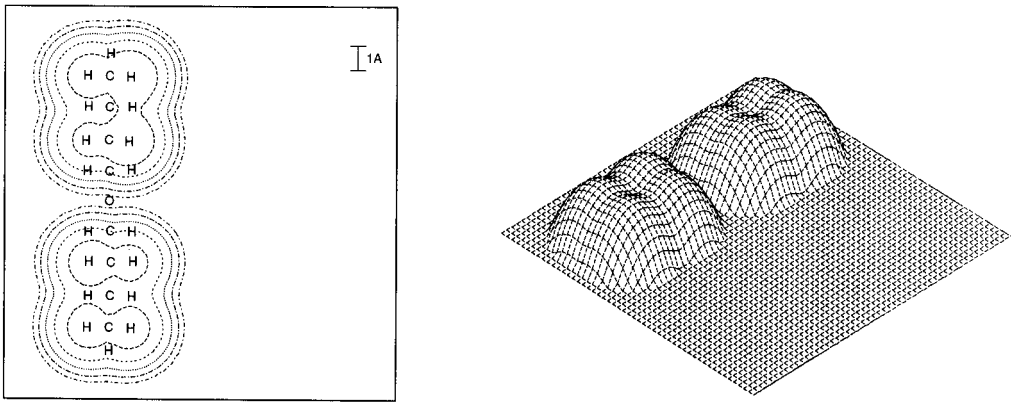

Figure 9. Computed constant current STM images of $CH_3(CH_2)_3O(CH_2)_3CH_3$ on graphite: (A) vertical orientation with the oxygen atom pointing down; (B) flat orientation; (C) vertical orientation with the oxygen atom pointing up. The maximum values for the three plots are 2.12, 1.51, and 1.76 au, respectively.

to effect a large and diagnostic change in the STM image. Although the Br is dark relative to the alkyl chain in a *trans*-conformation, it is predicted to be bright in both *gauche*-conformations. With the Br down, the Br pushes up one of the hydrogen atoms on the α carbon, and this topographic effect causes the α hydrogen atom to become bright in an STM image (Figure 6A). With the Br up, the Br atom itself is bright (Figure 6B). Neither of these predictions correspond to the experimental data on the alkanol bromide, which are instead in accord with the computational prediction that the more energetically stable *trans*-conformation is being imaged in the STM experiment. The prediction that a bromide group would change from dark to bright in an STM image if its conformation changed from *trans* to *gauche* is consistent with the image-contrast reversal

$$CH_3(CH_2)_3S(CH_2)_3CH_3$$

(A) Vertical, S down

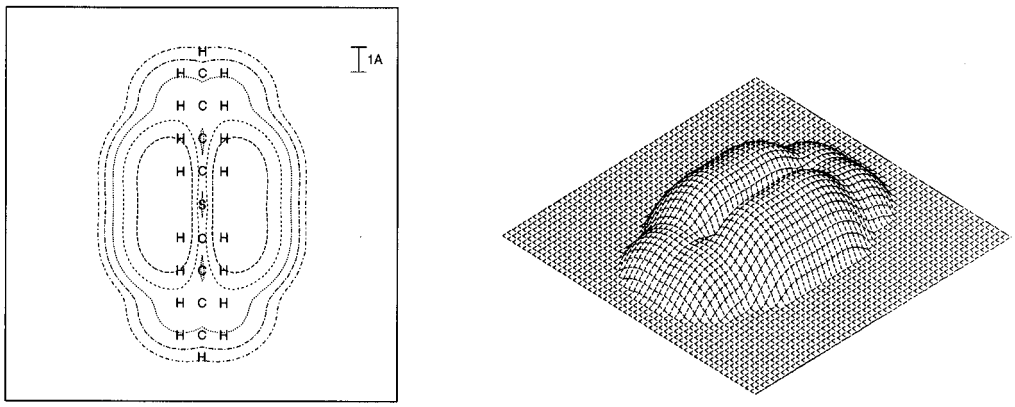

(B) Flat

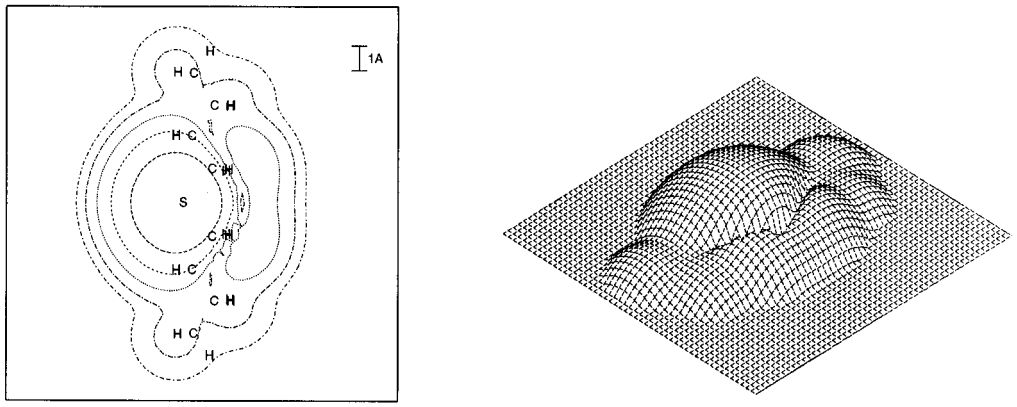

(C) Vertical, S up

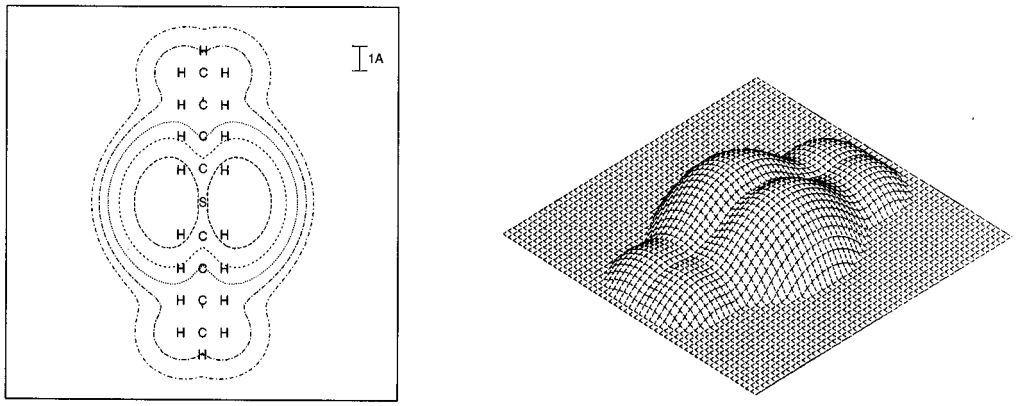

Figure 10. Computed constant current STM images of $CH_3(CH_2)_3S(CH_2)_3CH_3$ on graphite: (A) vertical orientation, with the sulfur atom pointing down; (B) flat orientation; (C) vertical orientation with the sulfur atom pointing up. The maximum values for the three plots are 3.17, 4.26, and 3.74 au, respectively.

that has been recently reported for bromide groups after sustained imaging of alkyl bromide overlayers on graphite substrates.[3]

III.D. Fluorinated Alkanols. Figures 7 and 8 depict the STM images that were computed for the CF_3 and C_3F_7 functional groups. Both of these molecules were considered in the flat adsorption orientation. As observed experimentally, both of these functional groups appear darker than the alkyl chain.

In these molecules, some fluorine atoms are closer to the tip than any other atom in the alkyl chain. Despite this topographic effect that should cause the flourine atoms to be bright in the

$$CH_3(CH_2)_3SH$$

(A) Flat

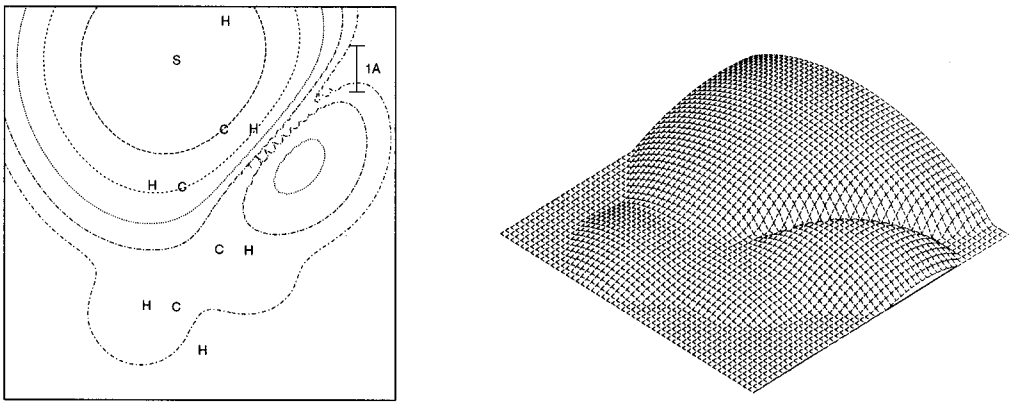

Figure 11. Computed constant current STM images of $CH_3(CH_2)_3SH$ laid flat on graphite. The maximum value for the plot is 4.30 au.

STM contrast, they are dark both theoretically and experimentally. This electronic effect results from the fact that the occupied orbitals describing the wave function in the fluorine region are computed to be very strongly bound, while the virtual orbitals are very far above the vacuum level. Hence, the current due to these orbitals is very small, despite a good overlap with the tip wave function, and these functional groups thus appear to be dark in STM contrast.

III.E. Ethers. The adsorption orientation on a graphite surface was determined for the long chain ether $CH_3(CH_2)_{15}$-$O(CH_2)_{15}CH_3$. According to FF simulations, a single molecule prefers to be adsorbed in the flat orientation, and the vertical orientations are computed to be less stable by 9.3 and 9.5 kcal/mol when the oxygen is pointing down and up, respectively. When the molecules are packed with a density close to the experimental one, the vertical orientation with oxygen pointing up is computed to be the most stable, followed by the vertical orientation with oxygen pointing down (1 kcal/mol) and the flat (8.2 kcal/mol) orientation. STM images for all three possibilities were therefore simulated.

Figure 9 reports the results obtained for a bias of -1 eV for the molecule $CH_3(CH_2)_3O(CH_2)_3CH_3$. In the vertical orientation with the oxygen down (Figure 9A), the ether is bright, due to the hydrogens on the α carbons. This image is thus not in agreement with experiment.

In the flat orientation (Figure 9B), the ether is dark and it appears similar to a missing hydrogen in the alkyl chain. In the vertical orientation with the oxygen pointing up (Figure 9C), the ether is also dark. In this orientation, the dark area is bounded by the spots corresponding to the hydrogens on the β carbons with respect to the oxygen.

Since by itself the observed STM contrast does not distinguish between the flat and O up orientations, it would be useful to obtain independent support for the orientational assignment suggested above. Such support can be obtained by inspection of the molecular packing arrangement of the ether overlayer. As discussed in the previous article, the characteristic angle θ is expected to be 0° for the sterically favored packing arrangement in the flat orientation (cf. Figure 20b in the previous article) and is expected to be 16° for the sterically favored packing in the vertical orientation (cf. Figure 20a in the previous article). The option for producing $\theta = 26°$ arises from the flat orientation with an offset of adjacent molecules by the distance of one methylene unit. The experimental observation of $\theta = 26°$ for the ether packing arrangement in the experimental STM images[1] therefore provides additional support for the suggestion that the ether is adsorbed in the flat orientation on the graphite surface.

III.F. Thioethers and Thiols. The FF simulation predicts one molecule of $CH_3(CH_2)_{13}S(CH_2)_{13}CH_3$ to be most stable when adsorbed in the flat orientation, and the vertical orientations are predicted to be higher in energy by 7.8 (S down) and 8.8 (S up) kcal/mol. When more molecules are packed at the density observed experimentally, the vertical orientation with the sulfur pointing down becomes the most stable. The other vertical orientation is higher in energy by 6.9 kcal/mol, and the flat orientation is higher in energy by 9.2 kcal/mol. Since these orientations were close in energy, STM images were computed for molecules in all three adsorption orientations.

Figure 10 presents the STM images predicted for the molecule $CH_3(CH_2)_3S(CH_2)_3CH_3$ in each of the three orientations. In all three orientations the alkyl chains define a linear intramolecular axis, so inspection of the molecular shape alone does not allow identification of the orientation that is being observed experimentally in the STM image unless the position of the sulfur relative to the alkyl chain can be accurately resolved.

In all three orientations, the sulfur appears much brighter than any other portion of the molecule. The lone pair orbitals on the sulfur atom are in the conduction region and are responsible for most of the tunneling current. Under these conditions, the actual size of the bright spot is expected to depend strongly on the dimensions and the shape of the tip. However, for the constant experimental conditions assumed in the simulations, the size of the bright spot is different for the three orientations, being larger in the vertical orientation having the sulfur pointed toward the graphite. The bright spot in the various computed constant current STM images is approximately 10 Å (S down), 8.2 Å (flat), or 5.4 Å (S up), as compared to the experimentally observed value of 6.5−6.7 Å.[1] This comparison is very instructive, indicating that the large apparent width of the thioether functionality observed in the experimental images[1] can be naturally explained by the electronic structure of this molecule.

Because alkanethiols have also been recently imaged using STM, the images of alkanethiol overlayers were also modeled theoretically in this study. Only the flat adsorption geometry was considered for the molecule $CH_3(CH_2)_7SH$, and the STM simulation was conducted on the molecule $CH_3(CH_2)_3SH$. As displayed in Figure 11, the thiol group is overwhelmingly brighter than the rest of the molecule. This prediction is in good agreement with experimental results.[3] The brightness is due to

$$CH_3(CH_2)_3SS(CH_2)_3CH_3$$

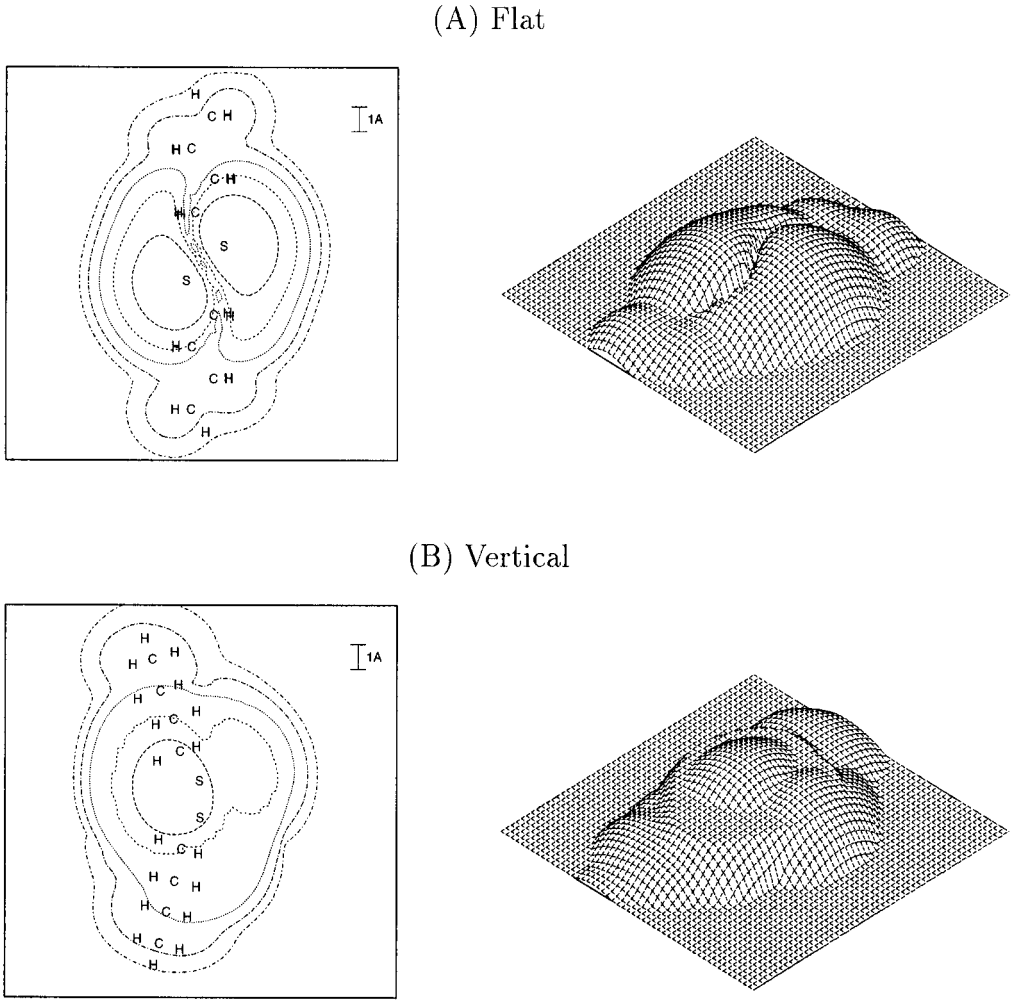

Figure 12. Computed constant current STM images of $CH_3(CH_2)_3SS(CH_2)_3CH_3$ on graphite: (A) flat orientation; (B) vertical orientation. The maximum values of the plots are 4.10 and 4.57 au, respectively.

the sulfur nonbonding electrons which enter the conduction region, making the thiol a conductor for the same reason that the S functionality is bright in the STM image of the thioether.

III.G. Disulfide. The molecule used to study the adsorption orientation is $CH_3(CH_2)_{15}SS(CH_2)_{15}CH_3$. Once again, for a single molecule, the flat adsorption orientation was computed to be favored, being lower in energy by 10.4 kcal/mol, while the vertical orientation is more stable by 7.9 kcal/mol for densely packed systems. Also, for this system, the lowest energy conformation of the vertical orientation of $CH_3(CH_2)_{15}SS(CH_2)_{15}CH_3$ had the carbon−carbon skeletons of both alkyl chains oriented perpendicular to the graphite surface plane. This adsorbate geometry is significantly different than the lowest energy molecular conformation for the disulfide in the gas phase, in which the carbon−carbon skeletons of the alkyl chains are mutually perdendicular. The STM predictions for the computed lowest energy flat and vertical orientations are reported for negative bias in Figure 12.

The computed images reveal that the disulfide functionality is much brighter than the rest of the molecule in either orientation. As discussed above for the iodoalkanol, the bright spot is due to the lone pair electrons on the sulfur, which become conducting electrons and thereby facilitate electronic coupling between the tip and the graphite. The apparent width of the disulfide functionality in the computed STM images is 9.4−11.3 Å, which is in good agreement with the experimentally observed value of 11.6− 12.6 Å. As is the case for the thioether, this agreement indicates that the very large width of the disulfide functional group in the experimental STM image has a very plausible physical explanation in terms of the electronic structure of the disulfide moiety.

III.H. Primary and Secondary Amines. Both primary and secondary amines have been imaged recently using STM. We first discuss the theoretical results for the secondary amine and then extend these findings to a primary amine.

For the secondary amine, four possible adsorption orientations must be considered: two flat and two vertical, with the amine hydrogen pointing either toward the graphite or away from the graphite. FF simulations on the molecule $CH_3(CH_2)_{17}NH(CH_2)_{17}CH_3$ predict isolated molecules to be more stable by 9.9 kcal/mol in the flat orientations and packed molecules to be more stable by 10.4 kcal/mol in the vertical orientations. Nevertheless, STM images were computed for all four orientations (Figure 13).

When the molecule is flat, the amine is predicted to be brighter than the rest of the molecule (Figures 13A,B). The brightness is localized on the hydrogen atoms which are close to the nitrogen and point toward the tip. The predicted brightness is due to the fact that the HOMO, which is localized on the amine, is in the conduction region, making the molecule a conductor.

$$CH_3(CH_2)_3NHCH_3(CH_2)_3$$

(A) Flat, NH up

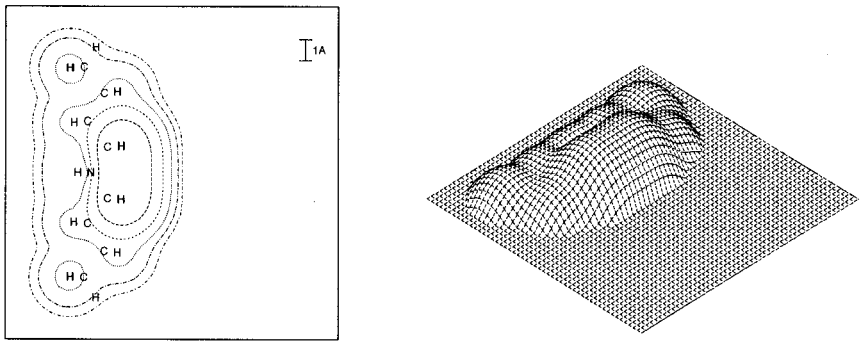

(B) Flat, NH down

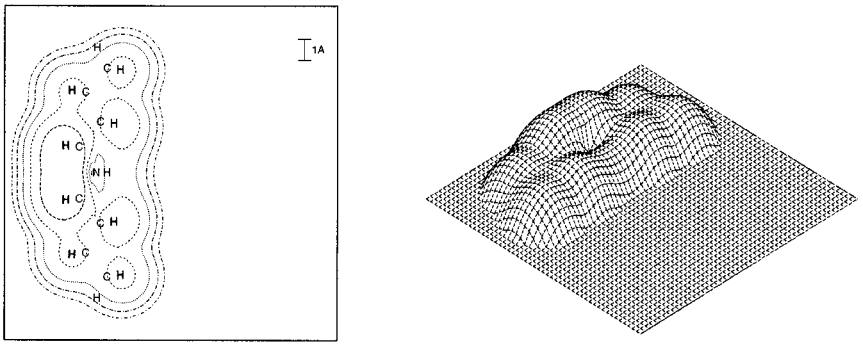

(C) Vertical, NH up

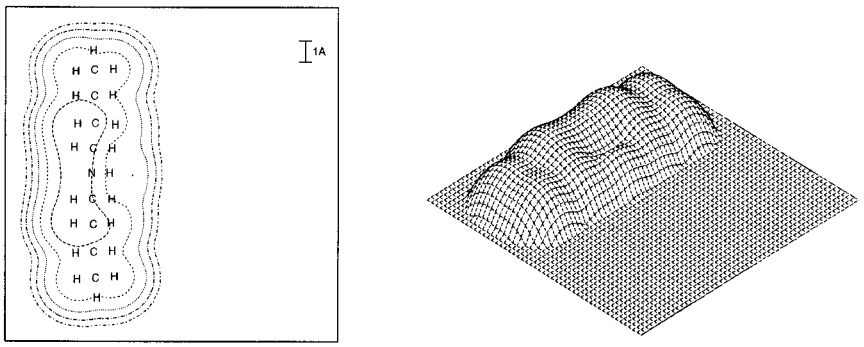

(D) Vertical, NH down

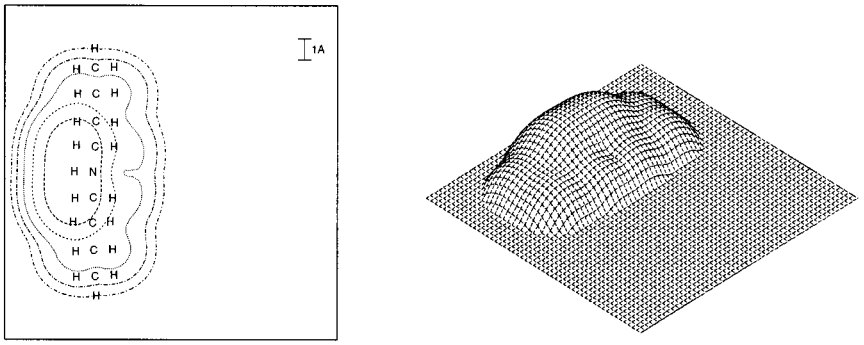

Figure 13. Computed constant current STM images of $CH_3(CH_2)_3NH(CH_2)_3CH_3$ on graphite: (A) flat orientation with the NH group pointing up; (B) flat orientation with the NH group pointing down; (C) vertical orientation with the NH group pointing up; (D) vertical orientation with the NH group pointing down. The maximum values for the plots are 2.71, 2.16, 2.26, and 3.00 au, respectively.

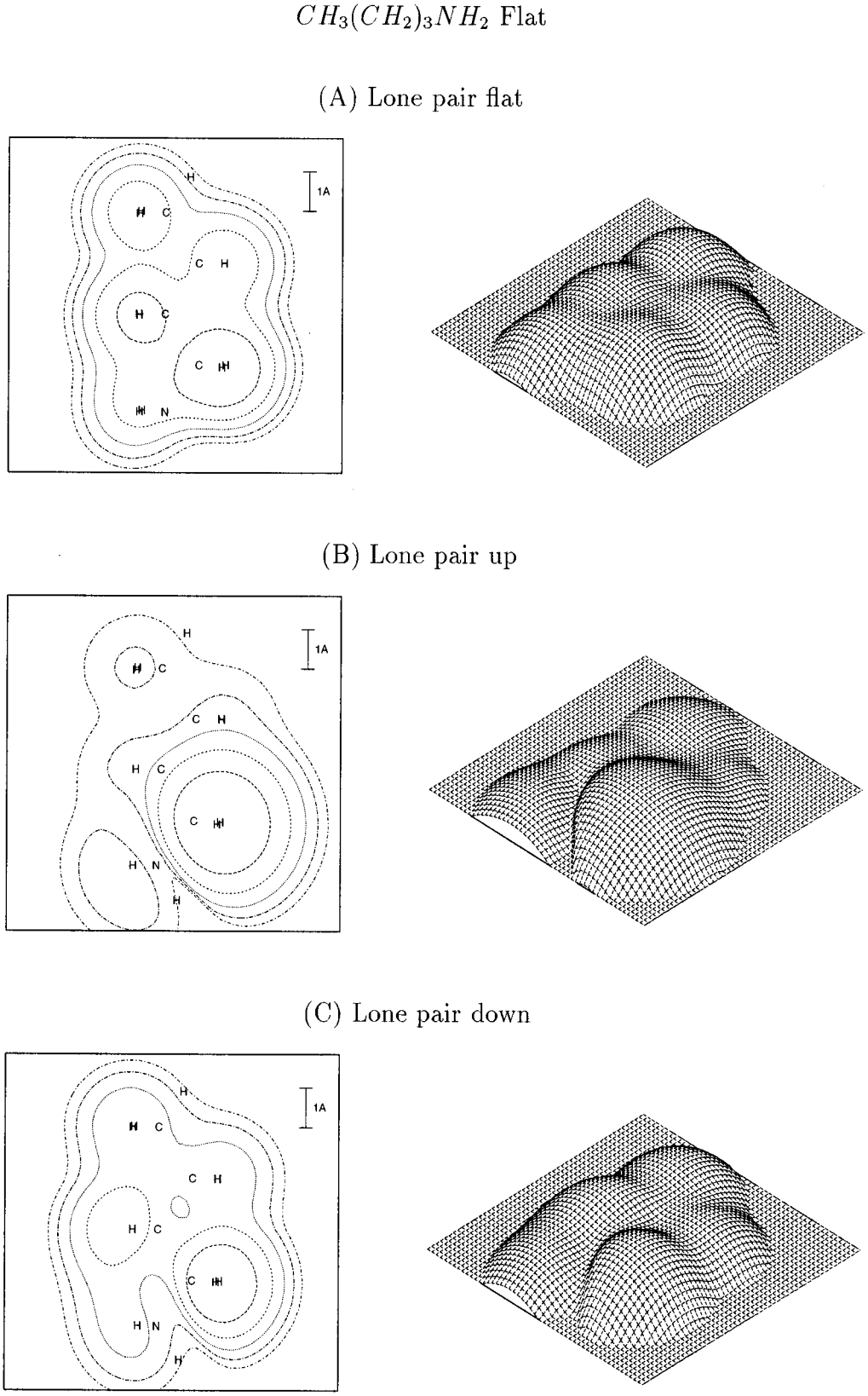

Figure 14. Computed constant current STM images of $CH_3(CH_2)_3NH_2$ adsorbed flat on graphite: (A) amine lone pair flat; (B) amine lone pair pointing up; (C) amine lone pair pointing down. The maximum values for the three plots are 1.39, 2.49, and 1.74 au, respectively.

When the molecule is vertical, the amine is only slightly brighter than the alkane chain when the NH group is pointing up (Figure 13C), and it is bright when the NH is pointing down (Figure 13D). The prediction is in qualitative agreement with the experimental image for three of the four possible orientations,[1] and further assignment cannot be made with the resolution of the STM data available at present.

To describe the properties of primary amines, the adsorption geometry of the molecule $CH_3(CH_2)_7NH_2$ was studied when the alkyl chain is flat. Three conformations were considered, in which the lone pair of the amine group was either flat (*trans* to the alkyl chain), pointing up, or pointing down. All three conformations are found to lie within 0.5 kcal/mol of each other and were investigated theoretically.

$$CH_3(CH_2)_3HC=CH(CH_2)_3CH_3$$

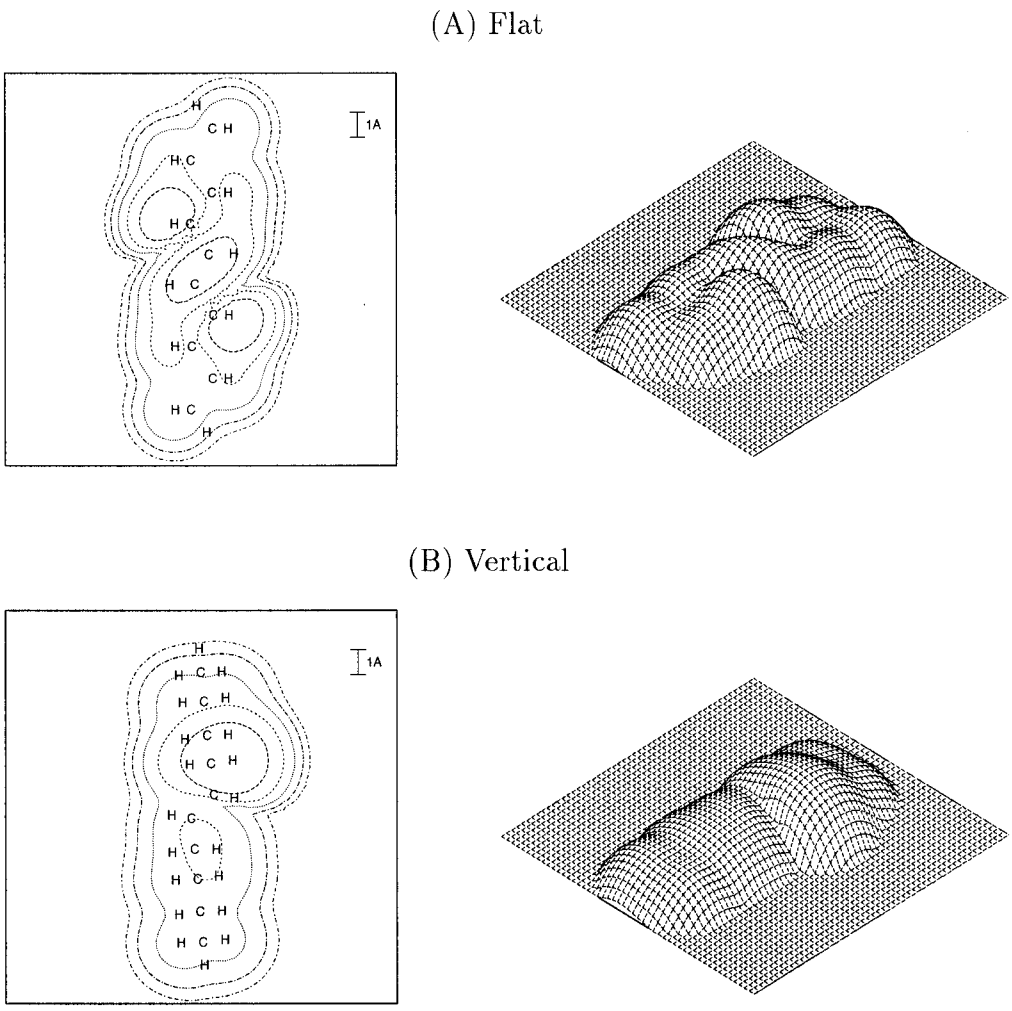

Figure 15. Computed constant current STM images of $CH_3(CH_2)CHCH(CH_2)_3CH_3$ on graphite: (A) flat orientation; (B) vertical orientation. The maximum values for the plots are 2.38 and 3.52 au, respectively.

The STM simulation was carried out on the molecule $CH_3(CH_2)_3NH_2$, and the results are reported in Figure 14. For all three conformations, the amine appears to be bright, with the main spot centered on the α hydrogens. This result is in qualitative agreement with the experimental images reported in the literature for a primary amine,[3] although the exact position of the bright spot could not be determined from the STM data on this system. The computations indicate that the low ionization potential of the amine brings the HOMO of the adsorbate into the conduction region. The HOMO has significant contributions from the α hydrogens, which have a good coupling with the tip and the graphite and appear therefore bright in the simulation.

III.I. Alkene. FF minimizations on the adsorbed molecule CH_3 $(CH_2)_{15}CHCH(CH_2)_{16}CH_3$ predict that isolated molecules should adsorb in the flat orientation, with the vertical orientation being more energetic by 9.1 kcal/mol. Packed molecules on the graphite surface are more stable by 11.8 kcal/mol in the vertical orientation, with the double-bond region strongly distorted toward a flat orientation and the rest of the molecule oriented vertically. We considered both orientations for the STM simulation.

The images obtained for *trans*-5-decene are reported in Figure 15. Both orientations exhibit a bright spot located close to the double bond, in agreement with the experimental results.[1] The high conductivity of this functionality in the STM experiment is due to the HOMO being located in the conduction region. In the flat orientation, the bright spot is centered on top of the double bond, essentially imaging the π system of the molecule (Figure 15A). In contrast to this electronic effect, in the vertical orientation the bright spot is dominated by topographical considerations and arises from the location of one of the hydrogen atoms pointing up from the molecule toward the tip (Figure 15B). Better resolution would be needed to distinguish between these possibilities experimentally.

Interestingly, the packing arrangement displayed by the *trans*-pentatriacontene produced an angle θ of 0° in the experimental STM images.[1] In this case, the possibility of significant intermolecular forces between the double bonds in the overlayer must be considered. Thus, for this system, the observed packing angle does not uniquely identify the orientation of the carbon−carbon skeleton, but it can be taken to indicate that the double bonds are in translational registry in the overlayer, as would be expected for significant $\pi-\pi$ interactions between adsorbed molecules.

III.J. Alkyne. The molecule studied experimentally by Claypool *et al.* is 7-hexadecyn-1-ol.[1] Since alkanols prefer to lie flat on the graphite,[1] only the flat orientation was investigated computationally.

The predicted image for 5-decyne, at a bias of −1 eV, is reported in Figure 16. In this image, the triple bond and the surrounding hydrogens appear to be brighter than the rest of

$$CH_3(CH_2)_3C \equiv C(CH_2)_3CH_3$$

(A) Flat

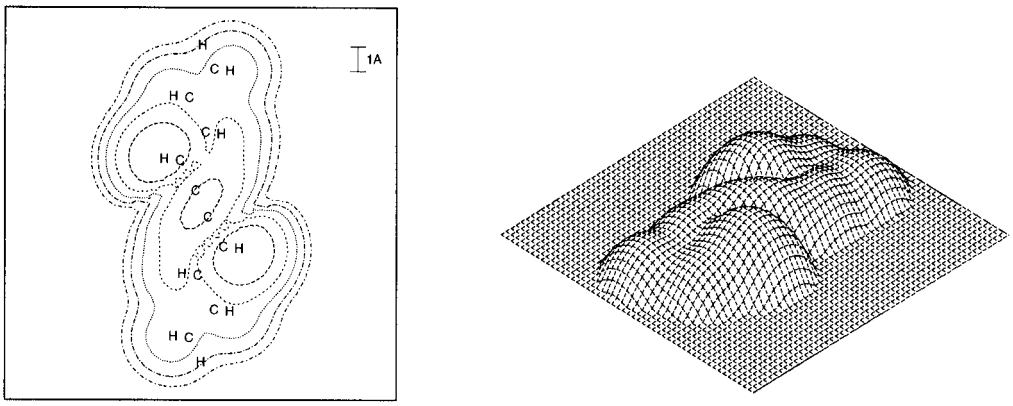

Figure 16. Computed constant current STM images of $CH_3(CH_2)_3CC(CH_2)CH_3$ laid flat on graphite. The maximum value for the plot is 2.58 au.

$$CH_3(CH_2)_3CN$$

(A) Flat

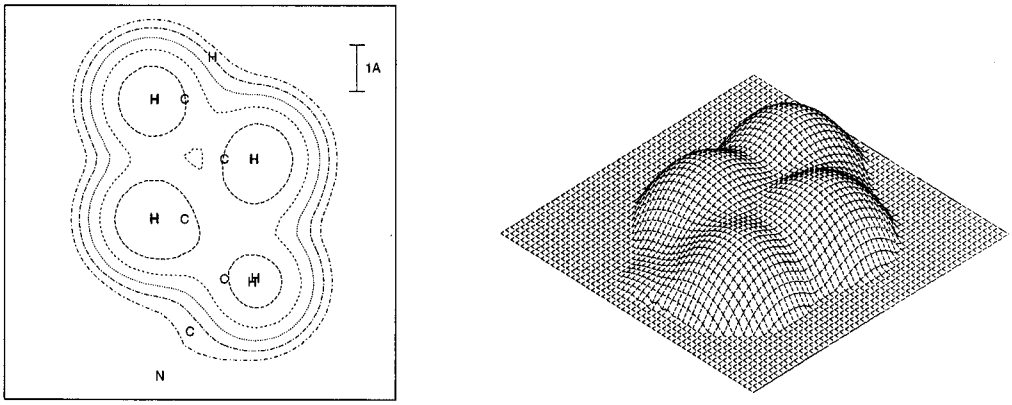

Figure 17. Computed constant current STM images of $CH_3(CH_2)_3CN$ laid flat on graphite. The maximum value of the plot is 1.09 au.

the molecule, in agreement with experimental data on 7-hexadecyn-1-ol[1] as well as on 10,12-octadecadiynoic acid.[4] The simulated width of the bright spot around the triple bond was 6.4 Å, vs the experimental observation of 3.5−4.3 Å.[1] Additionally, the flat orientation is expected to produce a kink around the triple bond due to the geometry of the molecule, and this feature is observed in the experimental STM images of the alkyne overlayers.[1]

III.K. Nitrile. Figure 17 depicts the predicted STM image of a nitrile. This functionality also has a π system, like the alkenes and alkynes discussed above, yet it appears dark in the experimental STM image.[1] This behavior is reproduced in the computed STM images. The nitrile HOMO is much lower in energy than that of the alkyl chain; additionally, in the energetically favored *trans*-conformation, the nitrile group is farther from the tip than are the methylene hydrogens in the alkyl chain. Thus, both electronic and geometric considerations would predict the group to be dark, in accord with the experimental STM data for nitrile-containing alkyl overlayers on graphite.[1]

III.L. Acid Dimer. Prior work has described STM images of carboxylic acids on graphite.[2,4] To investigate this system theoretically, the dimer $[CH_3(CH_2)_7COOH]_2$ was studied to determine the adsorption geometry. Only the adsorpion of one dimer was studied in the flat configuration.

The STM simulation was then performed on the smaller dimer $[CH_3(CH_2)_3COOH]_2$, and the results are reported in Figure 18. The acid region appears to be dark, in good agreement with the experimental results.[2] This occurs because, similar to the nitrile group, the π system of the acid group is very stable. The HOMO remains far from the conduction energy, and the image is dominated by the alkyl hydrogens, which are closer to the tip.

III.M. Ketone. FF simulations on the molecule $CH_3(CH_2)_{16}CO(CH_2)_{16}CH_3$ indicate that the flat orientation is expected to be most stable for a singly adsorbed molecule, while the vertical orientations with CO pointing down and up are 12.4 and 9.0 kcal/mol more energetic, respectively. For packing densities close to those observed experimentally, the vertical orientation with CO pointing up is most stable, the vertical orientation with CO poinitng down is less stable by 8.5 kcal/mol, and the flat geometry is less stable by 9.5 kcal/mol.

Figure 19 reports the computed STM images for $CH_3(CH_2)_3CO(CH_2)_3CH_3$ in each of the three orientations. The ketone region is bright in the STM image when the molecule is in the vertical orientation with the CO pointing down (Figure 19A). The brightness is predominantly topographic in origin and is due to the fact that the hydrogens closest to the CO are pushed toward the tip. In the flat orientation, the ketone is predicted to be dark (Figure 19B). The dark region extends over the

$(CH_3(CH_2)_3COOH)_2$

(A) Flat

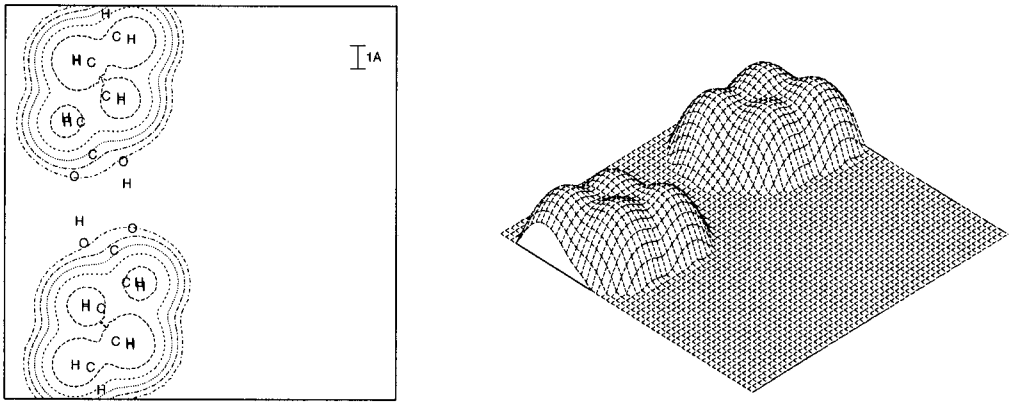

Figure 18. Computed constant current STM images of $[CH_3(CH_2)_3COOH]_2$ laid flat on graphite. The maximum value for the plot is 1.72 au.

hydrogens on the α carbons and, to a minor extent, to those on the β carbons with respect to the CO. In the vertical orientation with the CO pointing up, the ketone is predicted to be bright in the STM image (Figure 19C).

No conclusive experimental images are available for comparison with these computational results. Preliminary experimental data, however, gave a bright spot on the ketone for negative bias and a dark region for positive bias.[1] According to the theoretical model presented above for the effects of bias in STM experiments, based on the derivation of Marcus,[1,17] images obtained under positive and negative bias should be very similar unless the orientation or geometry of the molecule is different at the different bias polarities. Since the ketone is a polar group, it is possible that the transition from the flat to the vertical orientation with the CO pointing up is more favorable when the graphite has a negative charge (negative bias) than when the graphite has a positive charge. If this is the case, the observed images should depend on the history of the sample, with fresh samples having the molecules in the flat orientation and old samples, as well as samples already used for negative bias STM, having the molecules in the vertical orientation. These considerations are being investigated experimentally at present for ketones and for other highly polar functionalities adsorbed on graphite surfaces.

IV. Discussion

The predicted STM images reproduce the qualitative features of all of the experimental STM data reported in the accompanying article as well as those of other results on related systems.[1−5] These computations have provided physically reasonable explanations for the STM image contrast of all of the functional groups investigated experimentally and also allow an understanding of the widths of the various functional groups that have been observed in the experimental STM data.[1] In addition, the results explain the angles between the spots observed in the STM images of alkyl chains and in a number of cases allow assignment of the orientation of the adsorbates with respect to the graphite surface plane. The computations also allow separation of the importance of electronic and topographic effects in the STM images of many of the systems studied experimentally.

An interesting result arising from the computational model used in this work is the predicted importance of the virtual orbitals of the halogenated alkanols and of other related substituted alkanes in defining the STM image contrast. This result is different from the HOMO-dominated electronic coupling that is believed to determine electron tunneling matrix elements in intramolecular electron transfer processes between a donor and an acceptor connected to an alkane chain. The difference in importance of the occupied and virtual orbitals arises because the STM experiment is much more sensitive to the shape of the orbitals that are projected into the localized region defined by the tip−sample gap; thus, the more diffuse virtual orbitals can play a much more dominant role in defining the overall electronic coupling term in an STM experiment despite being significantly farther in energy from the Fermi level of the substrate than the occupied orbitals. Although the relative contributions of the virtual and occupied orbitals in determining electronic coupling matrix elements in an STM image have not been definitively established experimentally, the calculations presented herein should offer a framework for future experimental studies that are designed to evaluate these effects in a systematic fashion.

The computational results have allowed classification of the functional groups into three categories, based on how their electronic structure affects the contrast in an STM image. These categories are discussed briefly below.

IV.A. Conductors. These functional groups have an ionization potential lower than a fixed value I_0. The exact value of I_0 is not known, but on the basis of the available data it is between the ionization potential of an alkyl bromide and that of an alkyl amine.[1] These groups have one (or more) orbital, in resonance with the conduction states on the tip and on the graphite, that is responsible for most of the observed current. As the STM image is essentially a map of the conducting orbitals, these groups tend to appear much brighter than the alkyl chain. For functionalized alkanes on graphite, this category of functional groups includes disulfides, thioethers, thiols, amines, alkenes, alkynes, and alkyl iodides. This functional group classification is closely related to the HOMO−IP model discussed in the previous article.[1]

IV.B. Dark Groups. Functional groups that are not conductors and that have low electron affinities appear dark. This is because the coupling is small through both the HOMO and LUMO. In addition, the computations indicate that most of the tunneling current in the systems evaluated in this work is described by the low lying virtual orbitals, much like a low-energy electron diffraction process. Virtual orbitals, in fact, need to be orthogonal to the occupied orbitals. Since the occupied orbitals tend to be close to the nuclei, the virtual

$$CH_3(CH_2)_3CO(CH_2)_3CH_3$$

(A) Vertical, CO down

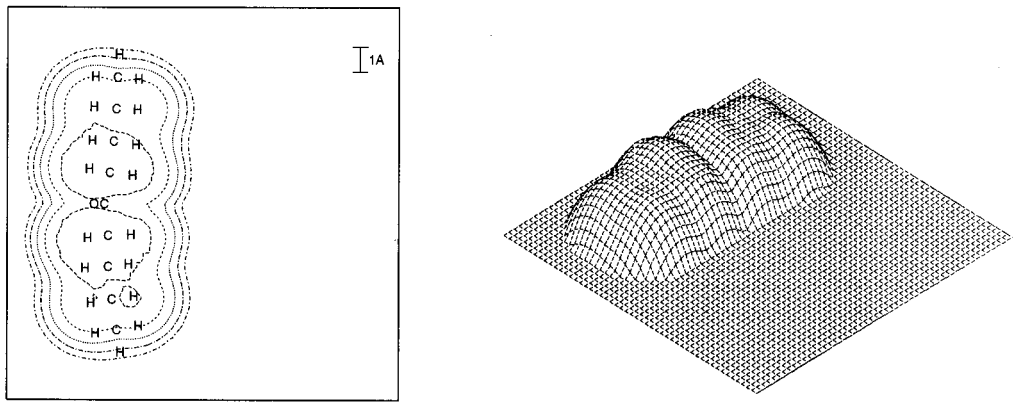

(B) Flat

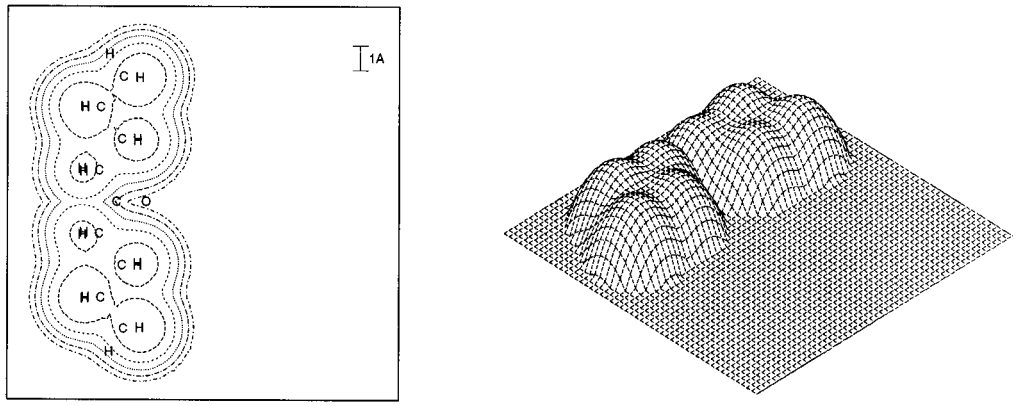

(C) Vertical, CO up

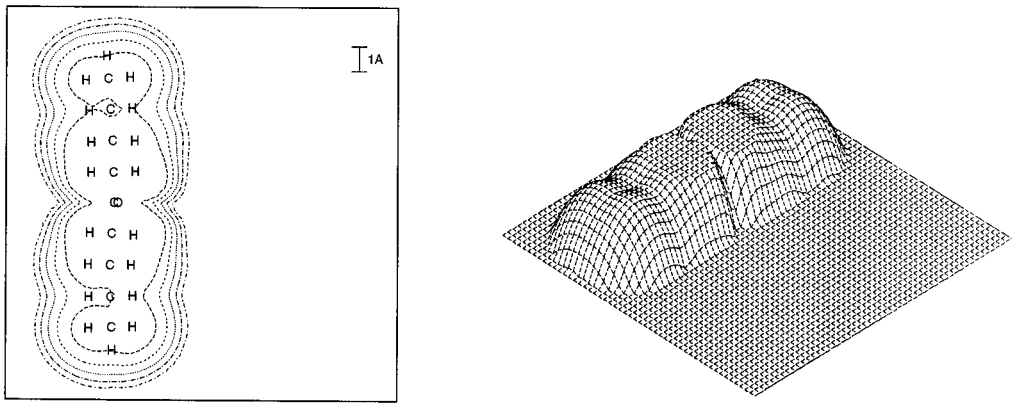

Figure 19. Computed constant current STM images of $CH_3(CH_2)_3CO(CH_2)_3CH_3$ on graphite: (A) vertical orientation with the CO pointing down toward the graphite; (B) flat orientation; (C) vertical orientation with the CO pointing up. The maximum values for the three plots are 2.23, 1.63, and 1.77 au, respectively.

orbitals are therefore squeezed toward the outside of the molecule and have better overlap, in general, with the tip and graphite, so they can dominate the tunneling matrix element that is responsible for the STM process. Functional groups with electron affinities lower than that of the corresponding alkane will hence be dark in the STM image. Nonconducting functional groups in this class include *trans*-conformations of alkyl fluorides, alkyl chlorides, alkyl bromides, and alcohols, as well as ethers and trifluoromethylene units.

IV.C. Bright Groups. Functional groups with high electron affinities but that are not conductors are expected to be brighter than the alkyl chain. However, these groups are not expected to appear as bright as conductors. Since the the relative energies of the virtual orbitals localized on different parts of the molecule

must be compared, it is also important to consider that charge-withdrawing groups will lower the electron affinity of the alkyl chain, effectively shifting the reference intensity of neighboring groups that might be used to establish the STM image contrast of the functional group. No functional groups in this class have apparently been observed yet.

IV.D. Relative Importance of Geometric and Electronic Effects. Since the electronic coupling is determined strongly by the overlap of each orbital with the tip and the graphite, the geometry of the molecule plays a key role in determining the STM image. In fact, the theoretical STM images presented in this work reveal that the experimental STM data for most of the functionalized alkane overlayers investigated to date are dominated by topographic effects of the molecules in the overlayer. Functional groups that are close to the tip (or to the graphite) will thus tend to appear bright unless there are strong electronic effects that reduce the orbital overlap in this region of space. Fluorinated alkyls (Figure 7) provide an example of this interplay between topographic and electronic effects in determining the contrast of an STM image. A theoretical description of the image contrast of such systems therefore requires an evaluation of electronic and steric effects in a fairly detailed fashion.

The conclusion that most molecules are imaged through the virtual orbitals is consistent with the observation that at low bias the graphite is imaged while at high bias the molecules are observed. The long-range behavior of an electronic wave function in a Coulomb potential is described by[14]

$$\psi(\mathbf{r}) = f(\mathbf{r})\mathrm{e}^{-\chi r} \quad \chi = \sqrt{2|E|} \tag{19}$$

where $f(\boldsymbol{r})$ diverges at most like a polynomial. Therefore, in general, the occupied MOs of the absorbate decay faster than the orbitals of the substrate that have energies near the graphite Fermi level. These graphite orbitals, in turn, decay faster than the virtual MOs of the absorbate overlayer. It follows that if the occupied orbitals dominate the STM images at large distances, then they should also dominate the image at smaller distances. Thus, the experimental data, which show a transition from images of graphite at small tip−sample biases to images of the overlayer at large tip−sample biases, are in accord with the behavior expected for the situation where the virtual orbitals of the molecular overlayer dominate the electronic coupling in the tip−sample gap. This result is, however, only described qualitatively at present because the graphite states were omitted in our simulation method so that the description of the STM data at high bias could be obtained in a straightforward fashion.

IV.E. Expense of the Computational Methods. The computational methods were reasonably inexpensive to perform. The computational cost of each prediction can be roughly divided as follows: 40% to optimize the adsorption geometry, 55% to run the HF computation, and 5% to run the actual STM simulation. The overall computer (CPU) time on HP9000/735 workstations is on the order of 30 min for the small molecules and 1 h for the largest ones. Thus, this theoretical framework can be readily adopted by a variety of researchers in order to guide future experimental investigations of the mechanisms underlying the image contrast of molecules in an STM experiment. Numerous theoretical predictions have been advanced in this article that will be interesting to explore experimentally, and the hope is that this set of predictions will stimulate experimental studies designed to elucidate further the factors that control these interesting atomic-resolution imaging processes.

V. Summary and Conclusions

In summary, a simple model, based on perturbation theory, was used to predict the STM images of molecules adsorbed on graphite. The geometries of the adsorbed molecules were estimated using a force field and the unperturbed molecular wave function was assumed to be the Hartree−Fock wave function for the gas-phase molecule, except for a simple shifting of the orbital energies to account for the fact that during the tunneling process the molecule is in close proximity to two conductors: the tip and the graphite.

The model contains one adjustable parameter representing the interaction between the molecules and the graphite. This parameter is expected to change very little for different molecules of the same family, and it was fixed to a value that seems to reproduce most of the experimental images.

For most of the molecules investigated in this study, topographic effects were observed to play a key role in determining the contrast observed in the experimental STM images. In fact, this correlation allows assignment of the orientation of most of the molecules with respect to the plane of the graphite surface and allows formulation of predictions regarding how the image contrast should be affected as the molecular orientation is varied. Electronic effects on the STM image contrast were revealed through an analysis of the orbital coupling properties of functional groups such as fluoromethyl and perflormethylene units in the alkane and alkanol overlayers investigated in this work.

The theoretical predictions are mainly qualitative, but they can provide significant insight into the experimental STM images and can define further avenues of interest in the experimental investigation of STM imaging mechanisms with a minor computational cost.

Acknowledgment. The research was funded by NSF (CHE 9522179 and ASC 9217368, W.A.G.; and CHE-9634152, N.S.L.). C.C. also acknowledges the NIH for a predoctoral training grant. The facilities of the MSC are also supported by grants from DOE-BCTR, Chevron Petroleum Technology Co., Asahi Chemical, Aramco, Owens-Corning, Asahi Glass, Chevron Research Technology Co., Chevron Chemical Co., Hercules, Avery-Dennison, BP Chemical, and the Beckman Institute.

Appendix A: Bias Dependence in Formulas (8), (16), and (18)

The bias dependence in eq 8 appears in two forms: (1) the integration domain is the conduction region CR defined as

$$\mathrm{CR} = \begin{cases} \{E{:}E \in (E_f, E_f + E_b)\} & \text{for negative bias } (E_b > 0) \\ \{E{:}E \in (E_f + E_b, E_f)\} & \text{for positive bias } (E_b < 0) \end{cases}$$

where E_f is the fermi energy and $-E_b$ is the bias; (2) the scaled orbital energies E_k are

$$E_k = \epsilon_k + \frac{1}{2}E_b$$

where ϵ_k is the original orbital energy.

We can write eq 8 as

$$I_{gt} = \frac{2\pi}{\hbar}\int_{E_f}^{E_f+E_b}\left|\sum_k \frac{V_{gk}V_{kt}}{\left(E - E_k - \frac{1}{2}E_b\right)}\right|^2 \rho_t(E)\,\rho_g(E)\,\mathrm{d}E$$

with the assumption that the absolute value of the integral be taken.

Including explicitly the dependence in eq 16 requires the definition of a new function $F(E)$:

$$F(E) = \begin{cases} 1 & \text{if } E \notin \text{CR} \\ 0 & \text{if } E \in \text{CR} \end{cases}$$

Equation 16 becomes then (again, we need to take the absolute value of the integral, but this time the relation is formally correct due to the $\propto$ symbol)

$$I \propto \int_{E_f}^{E_f+E_b} \rho_t(E)\rho_g(E)\left\{\left[\sum_k \frac{F\left(E_k+\frac{1}{2}E_b\right)V_{gk}V_{kt}}{\left(E-E_k-\frac{1}{2}E_b\right)}\right]^2 + \left[\pi\sum_k\left(1-F\left(E_k+\frac{1}{2}E_b\right)\right)V_{gk}V_{kt}\delta^{(\epsilon)}\left(E-E_k-\frac{1}{2}E_b\right)\right]^2\right\}\mathrm{d}E$$

Finally, eq 18 becomes

$$I \propto \int_{E_f}^{E_f+E_b}(E_f-E)^2\left[\sum_k \frac{F\left(E_k+\frac{1}{2}E_b\right)V_{gk}V_{kt}}{\left(E-E_k-\frac{1}{2}E_b\right)}\right]^2 + \int_{E_f}^{E_f+E_b}(E_f-E)^2\left[\pi\sum_k\left(1-F\left(E_k+\frac{1}{2}E_b\right)\right)V_{gk}V_{kt}\delta^{(\epsilon)}\left(E-E_k-\frac{1}{2}E_b\right)\right]^2\mathrm{d}E$$

References and Notes

(1) Claypool, C. L.; Faglioni, F.; Goddard, W. A., III; Gray, H. B.; Lewis, N. S.; Marcus, R. A. *J. Phys. Chem. B* **1997**, *101*, xxx.

(2) Liang, W.; Whangbo, M.-H.; Wawkuschewski, A.; Cantow, H.-J.; Magonov, S. N. *Adv. Mater.* **1993**, *5*, 817. Bar, G.; Magonov, S. N.; Cantow, H.-J.; Kushch, N. D.; Yabubskii, E. B.; Liang, W.; Ren, J.; Whangbo, M.-H. *New J. Chem.* **1993**, *17*, 439.

(3) Venkataraman, B.; Flynn, G. W.; Wilbur, J. L.; Folkers, J. P.; Whitesides, G. M. *J. Phys. Chem.* **1995**, *99*, 8684. Cyr, D. M.; Venkataraman, B.; Flynn, G. W.; Black, A.; Whitesides, G. M. *J. Phys. Chem.* **1996** *100*, 13747. Cyr, D. M.; Venkataraman, B.; Flynn, G. W. *Chem. Mater.* **1996** *8*, 1600.

(4) Rabe, J. P.; Buchholz, S. *Science* **1991**, *253*, 424. Rabe, J. P.; Buchholz, S.; Askadskaya, L. *Synth. Met.* **1993**, *54*, 339.

(5) Magonov, S. N.; Whangbo, M.-H. *Surface Analysis with STM and AFM*; VCH: New York, 1996.

(6) Tersoff, J.; Hamman, D. R. *Phys. Rev. Lett.* **1983**, *50*, 1998. Tersoff, J.; Hamman, D. R. *Phys. Rev. B* **1985**, *31*, 805.

(7) Bardeen, J. *Phys. Rev. Lett.* **1961**, *6*, 57.

(8) Lang, N. D. *Phys. Rev. Lett.* **1985**, *55*, 230. Lang, N. D. *Phys. Rev. Lett.* **1986**, *56*, 1164.

(9) Doyen, G.; Drakova, D.; Kopatzki, E.; Behm, R. J. *J. Vac. Sci. Technol. A* **1988**, *6*, 327. Kopatzki, E.; Doyen, G.; Drakova, D.; Behm, R. J. *J. Microsc.* **1988**, *152*, 687.

(10) Hallmark,V. M.; Chiang, S.; Meinhardt, K. P.; Hafner, K. *Phys. Rev. Lett.* **1993**, *70*, 3740. Hallmark, V. M.; Chiang, S. *Surf. Sci.* **1995**, *329*, 255.

(11) Sautet, P.; Joachim, C. *Chem. Phys. Lett.* **1991**, *185*, 23; *Surf. Sci.* **1991**, *271*, 387. Sautet, P.; Bocquet, M. L. *Surf. Sci.* **1994**, *304*, L445.

(12) Fisher, A. J.; Blöchl, P. E. *Phys. Rev. Lett.* **1993**, *70*, 3263.

(13) Yang, H. O.; Marcus, R. A.; Källebring, B. *J. Chem. Phys.* **1994**, *100*, 7814.

(14) Landau, L. D.; Lifshits, E. M. *Quantum Mechanics*; Pergamon Press: New York, 1977.

(15) Hehre, W. J.; Stewart, R. F.; Pople, J. A. *J. Chem. Phys.* **1969**, *51*, 2657.

(16) Koryta, J.; Dvorak, J.; Kavan, L. *Principles of Electrochemistry*, John Wiley & Sons Ltd.: New York, 1993.

(17) Marcus, R. A. *J. Chem. Soc., Faraday Trans.* **1996**, *92*, 3905.

(18) Landolt-Börnstein. *Numerical Data and Functional Relationships in Science and Technology* New Series; Springer-Verlag: Berlin, 1984; Group III, Vol. 13c. Charlier, J. C.; Gonze, X.; Michenaud, J. P. *Phys. Rev. B* **1991**, *43*, 4579.

(19) Mayo, S. L.; Olafson, B. D.; Goddard, W. A., III *J. Phys. Chem.* **1990**, *94*, 8897.

(20) Rappé, A. K.; Goddard, W. A., III *J. Phys. Chem.* **1991**, *95*, 3358.

(21) Morishige, K.; Takami, Y.; Yokota, Y. *Phys. Rev. B* **1993**, *48*, 8277.

(22) Frisch, M. J.; Trucks, G. W.; Schlegel, H. B.; Gill, P. M. W.; Johnson, B. G.; Wong, M. W.; Foresman, J. B.; Robb, M. A.; Head-Gordon, M.; Replogle, E. S.; Gomperts, R.; Andres, J. L.; Raghavachari, K.; Binkley, J. S.; Gonzalez, C.; Martin, R. L.; Fox, D. J.; Defrees, D. J.; Baker, J.; Stewart, J. J. P.; Pople, J. A. *Gaussian 92/DFT*, Revision F.4; Gaussian, Inc.: Pittsburgh, PA, 1993. Frisch, M. J.; Trucks, G. W.; Schlegel, H. B.; Gill, P. M. W.; Johnson, B. G.; Robb, M. A.; Cheeseman, J. R.; Keith, T.; Petersson, G. A.; Montgomery, J. A.; Raghavachari, K.; Al- Laham, M. A.; Zakrzewski, V. G.; Ortiz, J. V.; Foresman, J. B.; Peng, C. Y.; Ayala, P. Y.; Chen, W.; Wong, M. W.; Andres, J. L.; Replogle, E. S.; Gomperts, R.; Martin, R. L.; Fox, D. J.; Binkley, J. S.; Defrees, D. J.; Baker, J.; Stewart, J. P.; Head-Gordon, M.; Gonzalez, C.; Pople, J. A. *Gaussian 94*, Revision B.3; Gaussian, Inc.: Pittsburgh, PA, 1995.

(23) Pairler, G. E.; Pylant, E. O. *Science* **1996**, *272*, 1145.

(24) Lias, S. G.; Levin, R. D. *Ionization Potential and Appearence Potential Measurements, 1971−1981*; U.S. Department of Commerce/ National Bureau of Standards: Washington, DC, 1982.